Catalysts for High Cetane Ethers as Diesel Fuels

Final Technical Progress Report

For

September 1, 1998-August 31, 2001

Kamil Klier, Richard G. Herman, Heock-Hoi Kwon, James G. C. Shen,
Qisheng Ma, Robert A. Hunsicker, Andrew P. Butler, and Scott J. Bollinger

November 2002
Reissued in Disk Format March 2003

DOE Award Number DE-FG26-98FT40113-F

Submitted by

Lehigh University
Office of Research and Sponsored Programs
526 Brodhead Avenue
Bethlehem, PA 18015

for

Zettlemoyer Center for Surface Studies
and Department of Chemistry
Sinclair Laboratory, 7 Asa Drive
Lehigh University
Bethlehem, Pennsylvania 18015

Catalysts for High Cetane Ethers as Diesel Fuels

Disclaimer

This report was prepared as an account of work sponsored by an agency of the United States Government. Neither the United State Government nor any agency thereof, nor any of their employees, makes any warranty, express or implied, or assumes any legal liability or responsibility for the accuracy, completeness, or usefulness of any information, apparatus, product, or process disclosed, or represents that its use would not infringe privately owned rights. Reference herein to any specific commercial product, process, or service by trade name, trademark, manufacturer, or otherwise does not necessarily constitute or imply its endorsement, recommendation, or favoring by the United States Government or any agency thereof. The views and opinions of authors expressed herein do not necessarily state or reflect those of the United States Government or any agency thereof.

Catalysts for High Cetane Ethers as Diesel Fuels

ABSTRACT

A tungstena-zirconia (WZ) catalyst has been investigated for coupling methanol and isobutanol to unsymmetrical ethers, i.e. methyl isobutyl ether (MIBE) and compared with earlier studied sulfated-zirconia (SZ) and Nafion-H catalysts. In all cases, the ether synthesis mechanism is a dual site S_N2 process involving competitive adsorption of reactants on proximal acid sites. At low reaction temperatures, methylisobutylether (MIBE) is the predominant product. However, at temperatures >135EC the WZ catalyst is very good for dehydration of isobutanol to isobutene. The surface acid sites of the WZ catalyst and a Nafion-H catalyst were diagnosed by high resolution X-ray photoelectron spectroscopy (XPS) of N 1s shifts after adsorption of amines. Using pyridine, ethylenediamine, and triethylamine, it is shown that WZ has heterogeneous strong Brønsted acid sites. Theoretical study located the transition state of the alcohol coupling reaction on proximal Brønsted acid sites and accounted well for XPS core-level shifts upon surface acid-base interactions. While computations have not been carried out with WZ, it is shown that the SZ catalyst is a slightly stronger acid than CF_3SO_3H (a model for Nafion-H) by 1.3-1.4 kcal/mol.

A novel sulfated zirconia catalyst having proximal strong Brønsted acid sites was synthesized and shown to have significantly enhanced activity and high selectivity in producing MIBE or isobutene from methanol/isobutanol mixtures. The catalyst was prepared by anchoring 1,2-ethanediol bis(hydrogen sulfate) salt precursor onto zirconium hydroxide, followed by calcination to remove the $–(CH_2CH_2)–$ bridging residues.

Catalysts for High Cetane Ethers as Diesel Fuels

TABLE OF CONTENTS

	Page No.
Cover Page	1
Disclaimer	2
ABSTRACT	3
TABLE OF CONTENTS	4
LIST OF TABLES	6
LIST OF FIGURES	8
INTRODUCTION	11
EXECUTIVE SUMMARY	13
PART I: THE TUNGSTENA-ZIRCONIA CATALYST	
EXPERIMENTAL PROCEDURES	15
Catalyst Preparation	15
Catalyst Testing	15
Catalyst Characterization by Optical Spectroscopy	16
Catalyst Characterization by XPS	17
CATALYTIC RESULTS FOR THE WO_3/ZrO_2 CATALYST	20
Dehydration of Mixed Alcohols	20
Dehydration of Individual Alcohols	26
Temperature Effect on Selectivity	26
OPTICAL PROPERTIES OF THE CATALYSTS	33
Spectral Data and Analysis	33
Conclusions from Optical Spectroscopy	38

XPS STUDIES OF THE ACIDITY OF WO_3/ZrO_2 40

PART II: STUDIES OF THE ETHER SYNTHESIS NAFION-H CATALYST

XPS STUDIES OF THE ACIDITY OF THE NAFION-H CATALYST 46

MODELLING OF ETHER SYNTHESIS OVER NAFION-H 52

PART III: A NOVEL STRONG ACID CATALYST

DESIGN AND SYNTHESIS 56

CATALYTIC RESULTS 57

CONCLUSIONS 63

ACKNOWLEDGEMENTS 64

REFERENCES 65

LIST OF TABLES

Page No.

1. The Gaussian fitting results of the H_2O (v + *) combination bands and the mixed H_2O (2v) + OH (2v) overtone bands in the NIR regions of monoclinic zirconia, tetragonal SO_4-impregnated zirconia, and tetragonal WO_3-impregnated zirconia as determined by DRS. 37

2. The hydroxyl concentrations calculated from the diffuse reflectance spectra, given in monolayers, of monoclinic zirconia, tetragonal WO_3-impregnated zirconia, and tetragonal SO_4-impregnated zirconia. 38

3. Binding energies and intensities observed for the Zr and W XPS peaks for the clean W/Z catalyst. 42

4. Binding energies and intensities observed for the Zr and W peaks for the W/Z catalyst after evacuation at 150EC, adsorption of pyridine at ambient temperature, and evacuation at 150EC. 43

5. Binding energies and intensities observed for the Zr and W peaks for the W/Z catalyst after evacuation at 150EC, adsorption of ethylene-diamine (EDA) at ambient temperature, and evacuation at 150EC. 44

6. Binding energies and intensities observed for the Zr and W peaks for the W/Z catalyst after evacuation at 150EC, adsorption of triethylamine (TEA) at ambient temperature, and evacuation at 150EC. 46

7. Binding energies and intensities observed for the clean Nafion-H MicroSaddles (MS) catalyst after evacuation. 47

8. Binding energies and intensities observed for the Nafion-H MS catalyst after adsorption of ethylenediamine (EDA), with no thermal post-treatment. 49

9. Binding energies and intensities observed for the Nafion-H MS catalyst after adsorption of ethylenediamine (EDA), followed by thermal post-treatment of evacuation at 150EC. 51

10. Energetics of the dual-site S_N2 pathway M + B º TS º MIBE + W over sulfonic acid sites. 53

11. Energies (kcal/mol) of acid-base interactions and the SO!H!N distances (D) derived from the computational models. 55

12. Product space time yields (mol/kg cat/hr) in the reaction of

MeOH/i-BuOH (1:1 molar ratio) with flow rates of 3.44 mol/kg cat/hr alcohols and 16 mol/kgcat/hr carrier gas at 101.3 kPa total pressure over the $(HO)_3Zr\text{-}O_3SOCH_2CH_2OSO_3\text{-}Zr(OH)_3$-derived catalyst. 58

13. Product space time yields (mol/kg cat/hr) and selectivity (%) in the reaction of MeOH/i-BuOH (2:1 molar ratio) at 15.6 mol/kg cat/hr alcohols, 186 mol/kg cat/hr carrier gas and 175EC over the $(HO)_3Zr\text{-}O_3SOCH_2CH_2OSO_3\text{-}Zr(OH)_3$-derived catalyst. 61

LIST OF FIGURES

Page No.

1. Rates of MIBE formation from mixtures of methanol and isobutanol as a function of partial pressure of methanol, p_M, while keeping partial pressure of isobutanol, p_B, constant at 13 kPa (~), and p_B with constant p_M at 23 kPa ( ) over 1.0 g of the tungstena/zirconia (WZ) catalyst. The reaction conditions were 150°C, p_{total} =1360 kPa, and 18.7% N_2/He + alcohol feed rate of 125 mol/kg catalyst/h. Squares are experimental data and full lines are theoretical curves obtained by using Equation (7) for the dependence of v_{MIBE} on p_M and p_B with k_4 = 3.1 mol/kg/h, K_M = 0.010 kPa^{-1}, and K_B = 0.034 kPa^{-1}. 22

2. Langmuir-Hinshelwood linear plot for the dehydration of methanol and isobutanol to MIBE over 1.0 g tungstena/zirconia catalyst at 150°C, p_{total} = 1360 kPa, and 18.7% N_2/He + alcohol feed rate of 125 mol/kg catalyst/h. The slope and intercept give combinations of rate and equilibrium

   constants (a) $\%(K_M/(k_4K_B))$ = 0.309 and $(1 + K_bp_B)\ \%(k_4K_MK_B)$ = 43.8, with p_B = 13 kPa and varying the partial pressure of methanol p_M,

   and (b) $\%(K_B/(k_4K_M))$ = 1.05 and $(1 + K_mp_M)\ \%(k_4K_MK_B)$ = 37.95, with p_M = 23 kPa and varying the partial pressure of methanol p_B. k_4 is in mol/kg catalyst/h and K_M and K_B are in kPa^{-1}. 23

3. Langmuir-Hinshelwood linear plot for the dehydration of methanol and isobutanol to MIBE over 1.0 g tungstena/zirconia catalyst at 150°C, p_{total} = 1360 kPa, and 18.7% N_2/He + alcohol feed rate of 125 mol/kg catalyst/h. The slope and intercept give combinations of rate and

   equilibrium constants (a) $\%k_1$ = 1.08 and $(1 + K_Bp_B) / \%(k_1K_M^2)$ = 94.7

   and (b) $K_M\ \%(k_3K_B)$ = 0.066 and $(1 + K_bp_B) / \%(k_3K_B)$ = 4.39 where p_B =

   13 kPa and the partial pressure of methanol p_M was varied, and (c) $\%(K_B/k_3)$

   = 0.116 and $(1 + K_mp_M) / \%(k_3K_B)$ = 4.61 and (d) $K_B / \%(k_3K_Mp_M)$ = 0.122

   and $(1 + K_mp_M) / \%(k_1K_Mp_M)$ = 4.04, where p_M = 23 kPa and the partial pressure of methanol p_B was varied. k is in units of mol/kg catalyst/h and K_M and K_B are in units of kPa^{-1}. 25

4. Effect of methanol partial pressure (p_M) on the steady state rate of formation of DME over 1.0 g tungstena/zirconia at 127°C, p_{total} = 1360 kPa, and 18.7% N_2/He + alcohol feed rate of 125 mol/kg catalyst/h. 27

5. Effect of isobutanol partial pressure (p_B) on the steady state reaction rates for the major products, isobutene ( ) and isooctene ( ), over 1.0 g tungstena/zirconia at 127°C, p_{total} = 1360 kPa, and 18.7% N_2/He + alcohol feed rate of 125 mol/kg catalyst/h. 28

6. Langmuir-Hinshelwood linear plot for the dehydration of (a) methanol and (b) isobutanol over 1.0 g tungstena/zirconia catalyst at 127°C, p_{total} = 1360 kPa. The slope and intercept give combinations of rate and equilibrium constants (a) $1 / \%k_1 = 1.25$ for the two highest p_M data points and 2.06 for the two lowest p_M data points and $1 / \%k_1K_M = 91.3$ and 17.8, respectively, and (b) $\%(1 / (k_3K_B)) = 7.7$ and $\%(K_B / k_3) = 0.15$. k is in units of mol/kg catalyst/h and K_M and K_B are in kPa^{-1}. 29

7. Effect of temperature on the steady state reaction rates of MIBE (C), butenes (?), octene (>), and DME ( ) over 1.0 g tungstena/zirconia with methanol/isobutanol = 2/1 at p_{total} = 1360 kPa, and 18.7% N_2/He + alcohol feed rate of 125 mol/kg catalyst/h. 30

8. Arrhenius plots of the formation rates of the major products MIBE (C), butenes (?), octenes (>), and DME ( ) formed over the tungstena/ zirconia catalyst with methanol/isobutanol = 2/1 at p_{total} = 1360 kPa, and 18.7% N_2/He + alcohol feed rate of 125 mol/kg catalyst/h. 32

9. The diffuse reflectance spectra of monoclinic zirconia (m-ZrO_2), Tetragonal SO_4-impregnated zirconia (SO_4/t-ZrO_2), and tetragonal WO_3-impregnated zirconia (WO_3/t-ZrO_2) between 4,500 and 50,000 cm^{-1}. 33

10. DRS in the NIR region of monoclinic zirconia, tetragonal SO_4-Impregnated zirconia, and tetragonal WO_3-impregnated zirconia in the spectral range of 4,500 and 8,000 cm^{-1}. Peak positions are labelled, but accurate calibration needs to be carried out. 34

11. The NIR-DRS spectra of the hydroxyl absorption region for monoclinic zirconia and tetragonal tungstated zirconia on the same relative scale, along with the magnified difference spectrum obtained for the latter sample. 35

12. XPS survey spectrum of the W/Z catalyst. 41

13. XPS spectrum of the N 1s peak for the W/Z catalyst after evacuation at 150EC, adsorption of pyridine at ambient temperature, and evacuation at 150EC. The resolved peaks (solid lines) are fitted to the experimental data points. 43

14. XPS spectrum of the N 1s peak for the W/Z catalyst after evacuation at 150EC, adsorption of ethylenediamine at ambient temperature, and evacuation at 150EC. 44

15. XPS spectrum of the N 1s peak for the W/Z catalyst after evacuation at 150EC, adsorption of triethylamine (TEA) at ambient temperature, and evacuation at 150EC. 45

16. XPS N 1s spectrum of Nafion-H MS after adsorption of ethylenediamine (EDA), with no thermal post-treatment. 48

17. XPS N 1s spectrum of Nafion-H MS after adsorption of ethylenediamine (EDA), followed by a thermal post-treatment at 150EC. 50

18. The dual site TS structure for the MeOH + i-BuOH ° MIBE + H_2O reaction pathway showing **(A)** the F-TS orbital and **(B)** the B-TS orbital as the methyl group of MeOH moves toward forming the ether linkage. The atoms represented by colors are: red for O, gray for H, black for C, green for F, and blue for S. 54

19. The effect of i-BuOH addition on DME (●) and MIBE (■) production. The abscissa axis is the partial pressure $P_{\text{I-BuOH}}$ in kPa at a constant Pressure of methanol P_{MeOH} = 8.97 kPa. The ordinate axis expresses the rates of DME, v_{DME}, and MIBE, v_{MIBE}, in mol/kg cat/hr. 59

INTRODUCTION

Methanol and isobutanol are the predominant products formed from CO/H_2 synthesis gas over alkali-promoted Cu/ZnO-based (low temperature) catalysts [1-5], as well as over copper-free alkali-promoted (high temperature) oxide catalysts [6,7]. Since the two alcohols are produced together, their direct coupling to synthesize ethers for a number of applications is of interest. One such ether is the unsymmetrical methyl-isobutyl ether (MIBE) that has desirable characteristics as a fuel (cetane number = 53 [8]), and thus, can be employed as an additive to or as a neat fuel to substitute for current diesel fuels [9,10]. MIBE formed by the direct coupling of methanol-isobutanol (Equation 1) was previously investigated over a number of solid acid catalysts [11-13].

$$(CH_3)_2CHCH_2OH + CH_3OH \rightarrow (CH_3)_2CHCH_2OCH_3 + H_2O \qquad (1)$$

Improvement of product yields, particularly over inorganic oxides, was found to be desirable. Furthermore, if new catalysts were found for selectively converting isobutanol to isobutene, Equation 2, a chemical route to isobutene from natural gas or coal-derived synthesis gas would be provided [8].

$$(CH_3)_2CHCH_2OH \rightarrow (CH_3)_2C{=}CH_2 + H_2O \qquad (2)$$

Such a process would alleviate isobutene dependence on petroleum feedstock. Kinetic analyses [12,14] suggested that the mechanism of Reaction 1 is the S_N2 pathway involving competitive adsorption of reactants on proximal dual Brønsted acid sites on the catalyst surface, while that of Reaction 2 has been proposed to be an E2 reaction [11-13]. Reactions 1 and 2 are a specific implementation of a general class of dehydrocondensations and dehydrations occurring in a light alcohol + heavier C_2-branched primary alcohol mixture.

Dehydrocondensation of two different alcohols takes place over solid acid catalysts either as a concerted S_N2 reaction [12,13,15-18] or as a two-step, less efficient process involving carbenium chemistry [8]. The distinction between the two pathways was determined in this laboratory by ^{18}O retention [13,16], chirality inversion [16,18], and structure of the product isomers [16,17]. Side reactions resulted in symmetrical ethers and olefins *via* dehydration of the C_2+ alcohols, in particular branched alcohols.

Over sulfonic acid Nafion-H resin, it was shown by us that methanol (MeOH) and isobutanol (i-BuOH) react fairly selectively to form methyl isobutyl ether (MIBE) from MeOH/i-BuOH = 1 at 0.1 MPa [16] and 2 at . 1.35 MPa [11,12] at temperatures between 87 and 117EC by a dominant S_N2 reaction pathway [16]. Oxide catalysts tend to require higher reaction temperatures to achieve appreciable conversions and to catalyze the formations of hydrocarbons, e.g. isobutene, rather than ethers [15].

The objective of this research was to develop scientific background of catalysts and processes for technological advancement in the production of high cetane ethers from alcohols and olefins for use as premium diesel fuels. This involved the goals of synthesizing dual-site and ternary-site strong acid heterogeneous catalysts for activating and coupling alcohols to form ethers. The catalysts need to be selective, operate under mild reaction conditions, and economically produce diesel fuels and additives that have high cetane numbers. This was achieved by preparing, characterizing, and testing solid acid catalysts, with both experimental and computational methodologies employed to delineate active sites.

EXECUTIVE SUMMARY

In the first part of this report, catalyst formation, activity, selectivity, kinetics, and nature of active sites of the tungstena-zirconia (WZ) catalyst are described in detail, and it is now shown that this catalyst is active for ether synthesis from alcohols, specifically formation of high cetane methyl isobutyl ether (MIBE) *via* methanol/isobutanol coupling. This catalyst system had been explored previously for hydrocarbon isomerizations by Santiesteban et al. [19] at Mobil Technology Co. The specific reaction is that of MeOH + i-BuOH, which gives rise at low temperature (#127EC), in order of selectivities and abundances, to methyl-isobutyl ether (MIBE) > isobutene (IB) > isooctene (IO) > dimethylether (DME) >> methyl-tertiarybutyl ether (MTBE). X-Ray photoelectron spectroscopy (XPS) studies using amine bases indicate that the surface concentration of the accessible acid sites on the WZ catalyst is lower than expected from the tungstate content and are more diluted than observed with the Nafion-H catalyst. In addition, the Brønsted acid sites on the WZ catalyst are heterogeneous since stronger amine bases detect more acid sites. In the near-infrared (NIR) spectral region, the diminished intensity of the OH frequencies upon surface impregnation of the zirconia with tungstate indicates bonding of the tungstate species to the surface of the zirconia *via* the surface hydroxyl groups and that it is spread on the surface.

In the second part of this report, XPS studies of the acidity of Nafion-H resin catalyst are described. Further evidence is presented that the amine bases titrate Brønsted acid sites and that the active sites on these catalysts are proximal strong Brønsted acid sites. In addition, the ether synthesis reaction over this catalyst has been computationally modeled,

and the transition state of the alcohol-to-ether reaction on the proximal dual Brønsted acid sites has been found. It was shown that the synthesis pathway involves adsorption of the alcohols by hydrogen-bonding on the active sites, concerted transfer of an activated methyl group to the isobutyl oxygen to form the ether while three protons transfer among the methanol and two sulfonic groups, including transfer of a proton in the opposite direction on the catalyst surface. For the synthesis of MIBE, the calculated transition state barrier from free reactants, $E^{\ddagger} - 16$ kcal/mol, is comparable to the experimental 15 kcal/mol obtained with Nafion-H.

In the third part of this report, the design and synthesis of a novel sulfated zirconia catalyst having proximal strong Brønsted acid sites is described. It is shown that this catalyst has enhanced catalytic acidity and high ether selectivity at low reaction temperatures, where the MIBE space time yield is enhanced by 78% over a conventional sulfated zirconia catalyst. The presence of even a small amount of isobutanol in a stream of methanol drastically decreased the formation rate of dimethylether, while greatly enhancing the formation of MIBE. Once again, the preferential adsorption of isobutanol on the acid sites is observed, in agreement with its greater basicity compared with methanol.

PART I: THE TUNGSTENA-ZIRCONIA CATALYST

EXPERIMENTAL PROCEDURES

Catalyst Preparation. The WZ catalyst was prepared according to the procedure described elsewhere for a refluxed, impregnated (R/IM) catalyst [19]. Hydrous zirconia was first prepared, which was thereafter calcined to form ZrO_2. This preparation was carried out by added aqueous 10 M NH_4OH dropwise to a stirred $ZrOCl_2$ aqueous solution to precipitate the hydrous zirconia (final pH .9). After filtering, the solid was washed with distilled water and dried overnight at 95EC. The solid was reslurried in excess water, the pH adjusted to .9.0 with 10 M NH_4OH, and refluxed overnight. After cooling, the solid was filtered, washed with water, and dried overnight at 95EC. The $Zr(OH)_4$ was then impregnated with an ammonium metatungstate [$(NH_4)_6H_2W_{12}O_{40}$CxH$_2$O] solution, air-dried at 95EC, and calcined at 825EC for 3 hr. This gave a solid containing nominal 15 wt% W loading and a surface area of 69 m^2/g after calcination, properties similar to the Mobil Technology Co. preparation with 16.9 wt% tungsten and area of 62 m^2/g [19].

Catalyst Testing. The alcohol coupling reaction was carried out in a downflow stainless steel tubular reactor operated in the differential regime, as described in our earlier study [12]. Typically, 1 g of catalyst diluted with approximately 5 ml of 0.8 mm Pyrex beads was placed in the middle of the reactor between plugs of Pyrex wool. The reactor void volume below and above the catalyst bed was filled with 5 mm Pyrex beads. A J-type thermocouple was inserted into the top of the catalyst bed using an axial stainless steel thermowell.

The reaction rates were typically measured at temperatures between 127EC and 150EC. A mixture of 17.8 vol% N_2 in He (Airgas Northeast, Inc.) was used as a carrier gas. The gas flow rate was controlled using a calibrated mass flow meter (Union Carbide, Model FM-4550). The reactants, methanol and isobutanol (99.9+%, Alfa), were fed separately as liquids to heated lines leading to the inlet port at the top of the reactor using two metering pumps (ISCO, Model 314). The reactants were vaporized in a preheated section of the reactor as they were mixed with the carrier gas before reaching the catalyst bed. The furnace had three heating zones, which provided for very good temperature control. The reactor pressure was controlled by a MightyMite back pressure regulator.

The exit gas stream from the reactor was analyzed by using an on-line Hewlett-Packard gas chromatograph (Model 5890, Series II), which was equipped with automated heated sampling valves. Product analyses were achieved with a Cpsil-5CB capillary column (Chrompack) using a thermal conductivity detector. No dehydration of alcohols was observed over a bed containing only Pyrex beads nor on the reactor walls at temperatures up to 150EC. Steady state activities over the catalysts were achieved within 2 hr of initiating alcohol injection and after changing the reactor temperature and alcohol feed rate. The catalyst performance was steady over a few hundred hours of testing. For kinetic studies, the total conversion was kept at less than 5% at 127EC and approximately 10% at 150EC. In this range, the system performs as a differential reactor.

Catalyst Characterization by Optical Spectroscopy. All measurements were made with a computer-controlled, scanning, double-beam Cary 5E spectrophotometer (Varian Instruments, Inc.) with diffuse reflectance accessory and extended sample chamber. The

integrating sphere was coated with polytetrafluoroethylene (PTFE).

Spectral data were stored on a PC disk and transformed using the Kubelka-Munk relation before being plotted. The diffuse reflectance theory yields quantitative results [20-22] for low absorbing, semi-infinite samples based on the Kubelka-Munk relation, i.e.

$$K/S = (1 - R_4)^2 / 2 R_4, \quad (3)$$

where K = the absorption coefficient of the sample, S = the scattering coefficient of the sample, and R_4 = the reflectance of the sample. Where needed, corrections at high absorbances are made [22]. The reflectances of the samples were measured between 4,500 and 50,000 cm^{-1}. The two spectral regions of principal interest are the NIR region between 4,500 and 8,000 cm^{-1} and the UV region between 10,000 and 50,000 cm^{-1}. The NIR region contains vibrational combination bands and overtones of hydrogen-containing species, e.g. hydroxyl groups, which is useful for quantitative analysis of materials with low electronic spectral background. The UV region includes electronic spectra and was used to characterize the optical band edges of the samples.

The surface-doped zirconia samples were dried at 115EC for 24 hr in a furnace, after which they were removed and allowed to cool in a positive-pressure, nitrogen-filled glove bag or box. The samples were then transferred into diffuse reflectance cells having 1 mm thick 2 cm radius circular Suprasil windows. The cells were closed using a conical rubber stopper and sealed with Mylar film.

Catalyst Characterization by XPS. X-Ray photoelectron spectroscopy (XPS) analyses of the WZ catalysts before and after adsorption of amines were carried out using the Scienta ESCA-300 high resolution photoelectron spectrometer at Lehigh University [23].

This instrument utilizes a rotating Al K" anode to generate an unpolarized 7.6 KW X-ray flux (hv = 1486.8 eV), which is monochromatized by seven toroidally bent quartz crystals. The detector system, consisting of a 300 mm mean radius hemispherical electron energy analyzer and a multichannel plate detector, provided an overall energy resolution of 0.27 eV, as determined by the Fermi level edge from Ag at room temperature. The detector's high sensitivity and energy resolution allows for the analysis of insulated samples. To improve the quality of resolution for non-conducting materials, a Scienta hot filament flood gun with an energy range of 0-10 eV is available to supply electrons for charge compensation.

For XPS analysis, the ZrO_2 and the W/Z catalyst were each pressed into pellet form on top of a rectangular piece of tin using a hydraulic ram press. The pellet was then secured onto an ESCA analysis stub by clamping the edges of the tin piece to the stub with screws. The stub with the sample was inserted into the fast entry chamber of the Scienta instrument and evacuated to pressures < 1 x 10^{-6} Torr. The stub was then transferred into the analysis chamber where the surface of the sample was scraped *in situ* (using a SiC edge) to remove any adsorbed impurities.

Both the survey and the high-resolution scans were performed on the clean ZrO_2 and W/Z surfaces, with the pressure in the analysis chamber on the order of 5 x 10^{-9} Torr. Survey scans were conducted with 300 eV pass energy, an incremental step size of 1 eV, and a 0.8 mm slit width. Scans of Zr 3d, O 1s, C 1s, W 4f, and N 1s spectral regions were conducted in a high resolution mode with 150 eV pass energy, an incremental step size of 0.05 eV, and a 0.8 mm slit width. The pass energy refers to the energy to which the kinetic energy of the emitted photoelectrons is retarded by a retardation voltage for detection by the analyzer. The

step size in turn refers to the energy step between each sweep of the retardation voltage. The slit width refers to the width of the slit located at the entrance of the detector. A larger slit width provides increased photoemission intensity with poorer resolution. Because the W/Z catalyst was non-conducting, a hot filament gun set at 1.3 eV was applied during the analysis to supply electrons for charge compensation and improve the resolution.

The adsorption of amines onto dehydrated W/Z (and Nafion-H microsaddles) was performed on a separate glass vacuum/adsorption system. Each dehydrated powdered sample was transferred into a glass reaction tube, which was connected *via* a Cajon ultra Torr tube connector to a port on the vacuum manifold having a Teflon/glass stopcock. The sample was evacuated to pressures on the order of 10^{-3} Torr prior to the adsorption of the amines. The amines were purified by a freeze/thaw technique using liquid nitrogen as coolant. The catalysts were exposed to the purified amines at room temperature and 15 Torr for 30 min. The catalysts were again evacuated to 10^{-3} Torr following the exposure. The adsorption system allowed for heating the catalyst before and/or after the adsorption treatment, where the latter provided for desorption of loosely adsorbed amines.

After the adsorption/evacuation treatment, the glass connecting tube between the stopcock and the vacuum system was break-opened, and the evacuated tube was moved to a nitrogen-filled glove bag or glove box. Opening the stopcock filled the tube with nitrogen, after which the tube was removed from the Cajon tubing connector, and the powdered sample was mounted on an ESCA analysis stub with the use of double sided sticking tape. The surface of the mounted sample was smoothed by using pressure applied from a smooth spatula. The prepared stub was transferred in a nitrogen-filled desiccator from the glove box

or bag to a glove bag attached to the entrance port of the Scienta ESCA 300 fast entry chamber. The chamber was brought to atmospheric pressure with nitrogen and the sample was transferred from the glove bag to the fast entry chamber. After sealing the fast entry chamber, it was evacuated to approximately 1 x 10^{-6} Torr, after which the sample was moved into the analytical chamber, which maintained a vacuum of approximately 10^{-9} Torr.

CATALYTIC RESULTS FOR THE WO_3/ZrO_2 CATALYST

Dehydration of Mixed Alcohols. A kinetic study was carried out with mixtures of methanol and isobutanol at a total reaction pressure of 1.36 MPa. In these studies, the partial pressure of one alcohol was maintained constant while the partial pressure of the other alcohol was varied. This allowed for determination of reaction rates and kinetic parameters for isobutanol dehydration to form isobutene (IB) and coupling reactions to form dimethylether (DME), diisobutylether (DIBE), and methylisobutylether (MIBE) using Equations (4)-(7).

$$v_{DME} = k_1 K_M^2 p_M^2 / (1 + K_M p_M + K_B p_B)^2 \quad (4)$$

$$v_{DIBE} = k_2 K_B^2 p_B^2 / (1 + K_M p_M + K_B p_B)^2 \quad (5)$$

$$v_{IB} = k_3 K_B p_B / (1 + K_M p_M + K_B p_B)^2 \quad (6)$$

$$v_{MIBE} = k_4 K_M p_M K_B p_B / (1 + K_M p_M + K_B p_B)^2 \quad (7)$$

In these equations utilized for determining the formation rates (v_i) of the products, p_M is the partial pressure of methanol, p_B is the partial pressure of isobutanol, the k_n values are the kinetic constants, and the K_n values are the adsorption equilibrium constants.

Results obtained at reaction temperatures of 127EC and 176EC are shown in Figure

1, which represents MIBE formation rates as a function of partial pressure of each reactant while keeping the pressure of the second alcohol constant. Symbols represent experimental data at 150°C and the full lines are theoretical curves based on Langmuir-Hinshelwood kinetics as described in Nunan et al. [12]. The MIBE formation rates show maxima in the dependence on partial pressures of both alcohols at both reaction temperatures, which implies optimum regime for the MIBE synthesis by either alcohol. The kinetic and adsorption equilibrium constants were obtained by fitting Equation (7) given above.

Figure 2 shows examples of using the linear forms of the rate laws, where (a) the partial pressure of isobutanol was maintained constant at 13 kPa while varying the methanol partial pressure and (b) methanol was maintained constant at 23 kPa while varying the isobutanol partial pressure. These linear plots yield the slopes and intercepts for experiments in which pM and pB were separately varied. The ratio of the intercept to the slope in each linear plot provided $(1 + K_B p_B) / K_M$ and $(1 + K_M p_M) / K_B$, respectively. Since p_M and p_B were set as constants, K_M and K_B could be determined unambiguously.

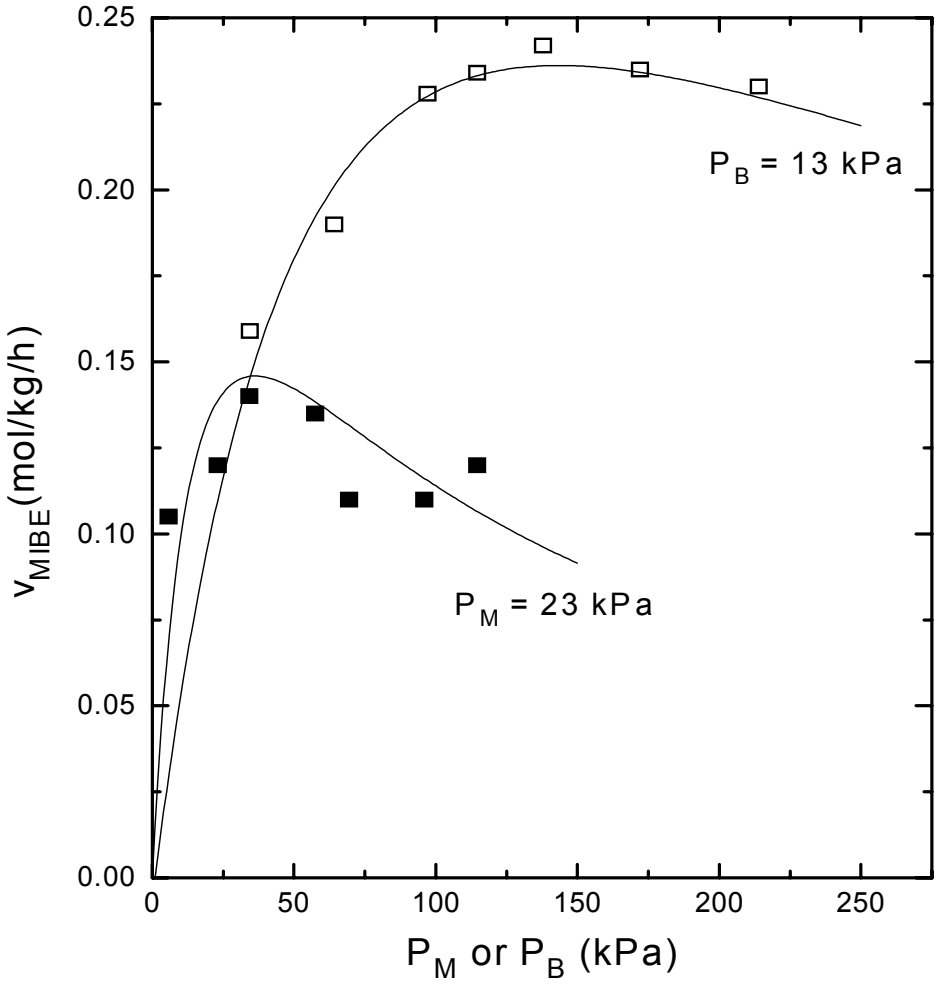

Figure 1. Rates of MIBE formation from mixtures of methanol and isobutanol as a function of partial pressure of methanol, p_M, while keeping partial pressure of isobutanol, p_B, constant at 13 kPa (~), and p_B with constant p_M at 23 kPa ( ) over 1.0 g of the tungstena/zirconia (WZ) catalyst. The reaction conditions were 150°C, p_{total} =1360 kPa, and 18.7% N_2/He + alcohol feed rate of 125 mol/kg catalyst/h. Squares are experimental data and full lines are theoretical curves obtained by using Equation (7) for the dependence of v_{MIBE} on p_M and p_B with k_4 = 3.1 mol/kg/h, K_M = 0.010 kPa^{-1}, and K_B = 0.034 kPa^{-1}.

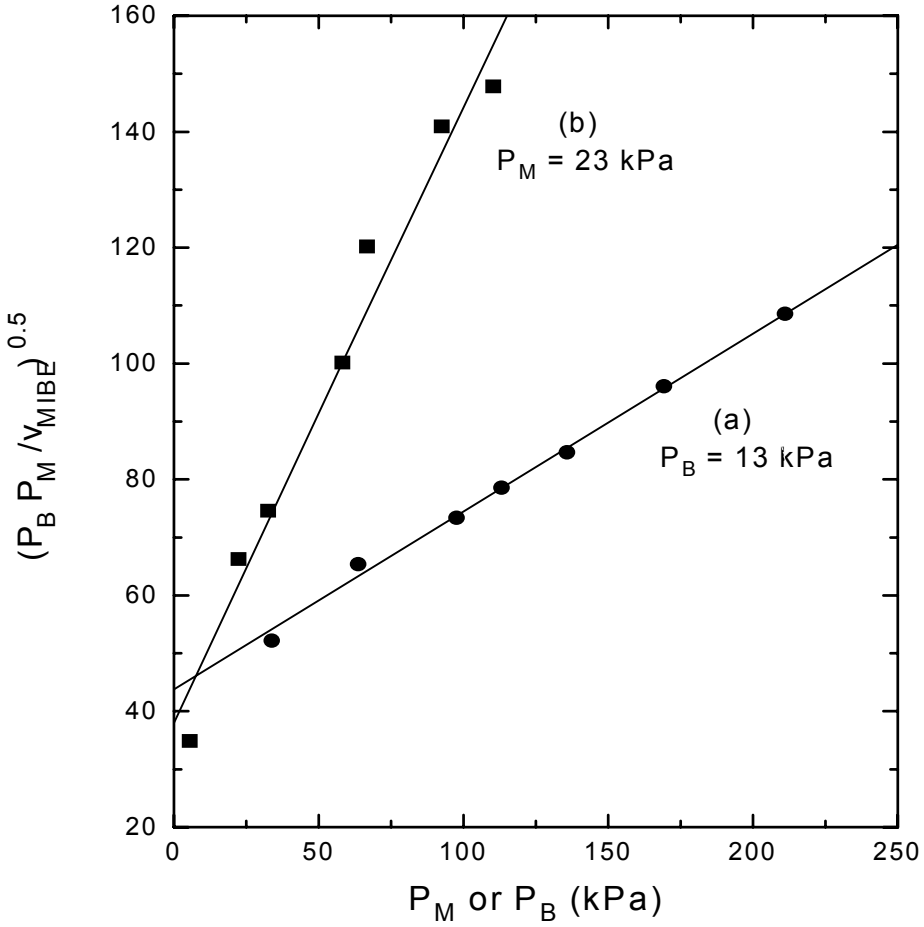

Figure 2. Langmuir-Hinshelwood linear plot for the dehydration of methanol and isobutanol to MIBE over 1.0 g tungstena/zirconia catalyst at 150°C, p_{total} = 1360 kPa, and 18.7% N_2/He + alcohol feed rate of 125 mol/kg catalyst/h. The slope and intercept give combinations of rate and equilibrium constants (a) $\%(K_M/(k_4K_B))$ = 0.309 and $(1 + K_b p_B)\ \%(k_4K_MK_B)$ = 43.8, with p_B = 13 kPa and varying the partial pressure of methanol p_M, and (b) $\%(K_B/(k_4K_M))$ = 1.05 and $(1 + K_m p_M)\ \%(k_4K_MK_B)$ = 37.95, with p_M = 23 kPa and varying the partial pressure of methanol p_B. k_4 is in mol/kg catalyst/h and K_M and K_B are in kPa^{-1}.

The kinetic and adsorption equilibrium constants were k_4 = 3.1 mol/kg/h, K_M = 0.010 kPa^{-1}, and K_B = 0.034 kPa^{-1} at 150°C. At 127°C, theoretical curves with k_4 = 0.93 mol/kg/h, K_M = 0.011 kPa^{-1}, and K_B = 0.039 kPa^{-1} successfully fitted the experimental data. The ratio of K_B/K_M was 3.4 at 150°C and 3.5 at 127°C, respectively, implying that isobutanol adsorbs more strongly to the active sites on the surface than methanol. Under similar reaction conditions (127°C and 1340 kPa), Nafion-H was reported to have the following constants: k_4 = 2.78 mol/kg/h, K_M = 0.0137 kPa^{-1}, K_B = 0.0243 kPa^{-1}, and K_B/K_M = 1.8 [12]. Although the constants are of the same order of magnitude, Nafion H turned out to be approximately 2.4 times more active for MIBE production than the present tungstena/zirconia catalyst.

With the rate constant obtained at 150 °C and activation energy (discussed later in this report) for MIBE formation, k_4 at 127°C could be determined from the Arrhenius rate expression, $k_4 = A \exp(-E_a/RT)$. The k_4 value was determined to be 1.04 mol/kg/h with a pre-exponential factor of $A = 5.7 \times 10^8$. This value of k_4 is very close to that determined from the separate experiment described above. In addition, the equilibrium constants K_B and K_M could also be determined from the data for DME and IB formation by using the linearized forms of Equations (4) and (6). The resulting linear plots in Figure 3 yield K_M = 0.015 kPa^{-1} and K_B = 0.037 kPa^{-1} (and k_4 = 2.7 mol/kg/h). The theoretical curves with the equilibrium and kinetic constants so obtained deviated appreciably from the experimental data and did not fit the experimental data as well as those shown in Figure 1. However, correct trends were predicted, and the values of K_B and K_M were not too different from those determined from the MIBE experiment (Figure 1), i.e. 0.034 and 0.010 kPa^{-1}, respectively.

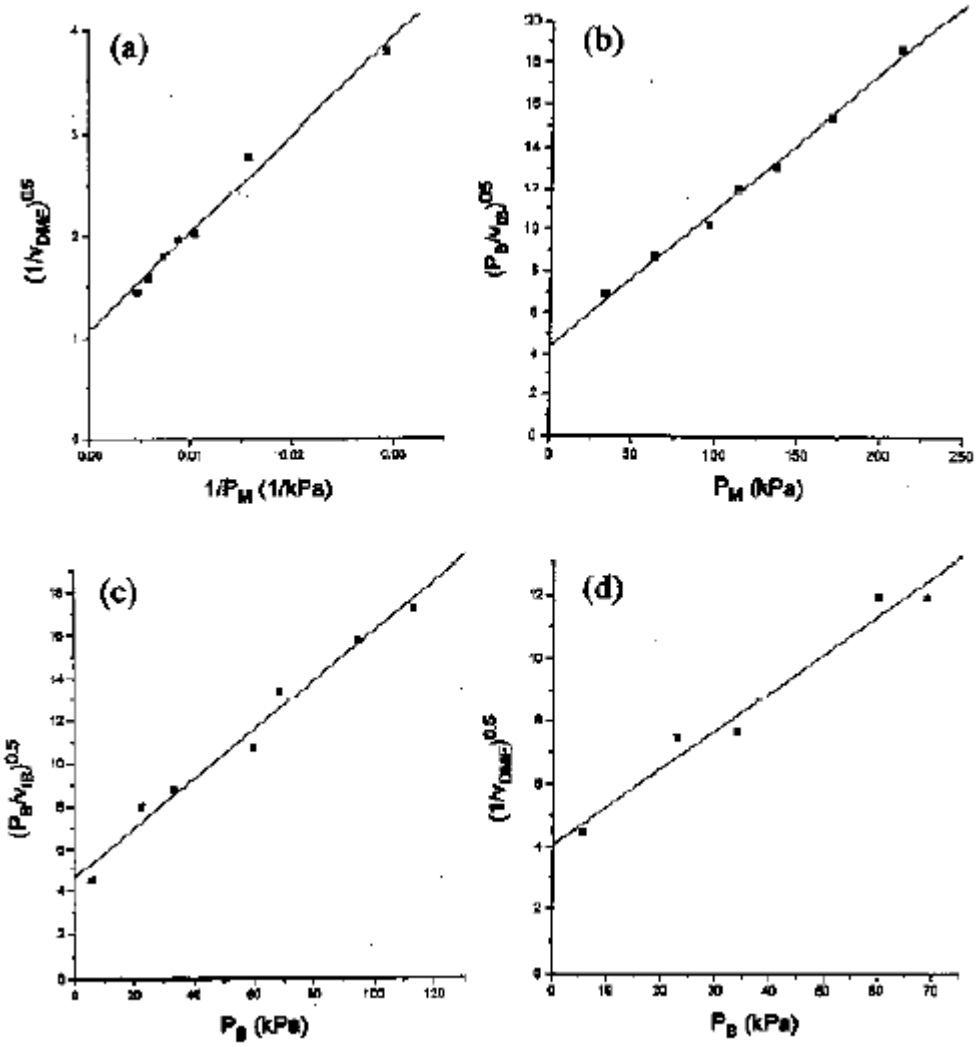

Figure 3. Langmuir-Hinshelwood linear plot for the dehydration of methanol and isobutanol to MIBE over 1.0 g tungstena/zirconia catalyst at 150°C, p_{total} = 1360 kPa, and 18.7% N_2/He + alcohol feed rate of 125 mol/kg catalyst/h. The slope and intercept give combinations of rate and equilibrium constants (a) $\%k_1 = 1.08$ and $(1 + K_B p_B) / \%(k_1 K_M^2) = 94.7$ and (b) K_M $\%(k_3 K_B) = 0.066$ and $(1 + K_b p_B) / \% (k_3 K_B) = 4.39$ where p_B = 13 kPa and the partial pressure of methanol p_M was varied, and (c) $\%(K_B/k_3) = 0.116$ and $(1 + K_m p_M) / \%(k_3 K_B) = 4.61$ and (d) $K_B / \%(k_3 K_M p_M) = 0.122$ and $(1 + K_m p_M) / \%(k_1 K_M p_M) = 4.04$, where p_M = 23 kPa and the partial pressure of methanol p_B was varied. k is in units of mol/kg catalyst/h and K_M and K_B are in units of kPa^{-1}.

Dehydration of Individual Alcohols. Experiments were also carried out using only one of the alcohols as a reactant at 127°C and p_{total} = 1360 kPa. In methanol dehydration in the absence of isobutanol, DME was the only reaction product observed, and the formation rate was leveling off at high methanol pressures (Figure 4). For isobutanol dehydration, isobutene and isooctene were the major products. The cis- and trans-2-butenes were observed as minor products, but no diisobutylether (DIBE), which is one of the significant products over Nafion H, was detected. The rates of formation of the major products formed from isobutanol are shown in Figure 5. Using the same graphical analysis methods as previously described, the plots shown in Figure 6 were obtained. The kinetic and equilibrium constants from this analysis of the reactions of the individual alcohols were determined to be in the same order of magnitude (K_M = 0.014-0.047 kPa^{-1} and K_B = 0.0196 kPa^{-1}). Although the K_M value from MIBE synthesis with mixed alcohols was within the range of the value of K_M obtained from the methonol-only experiment, the K_M value varied depending on p_M, implying failure of the Langmuir-Hinshelwood kinetic analysis based on Equation (4). Further data analysis will be carried out to obtain an explanation and/or a better kinetic equation.

Temperature Effect on Selectivity. In order to elucidate the effect of temperature on product selectivity over the tungstena/ zirconia catalyst, the reaction temperature was varied between 127°C and 150°C while keeping the total pressure constant at 1360 kPa. The reactant ratio methanol/isobutanol = 2 was maintained. The product selectivity as a function of temperature is shown in Figure 7. At 127°C, MIBE was the dominant product, but at

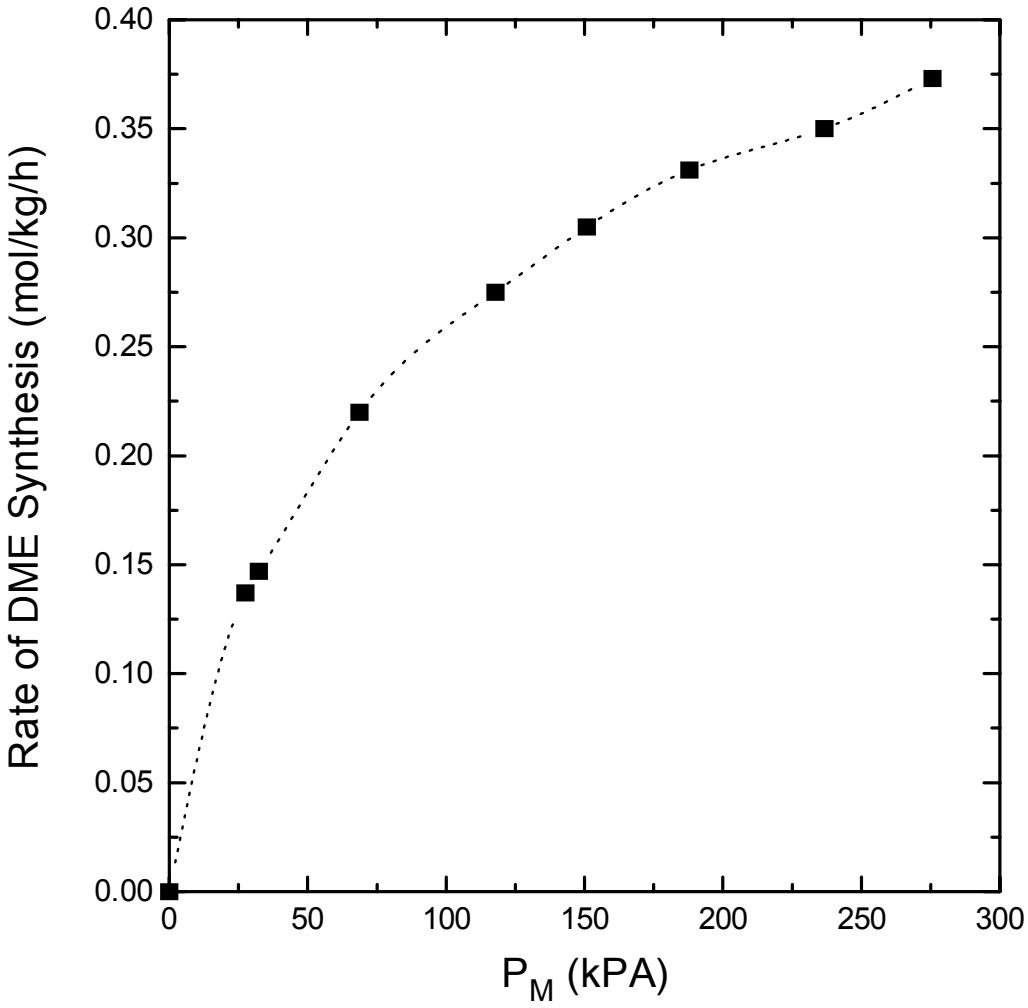

Figure 4. Effect of methanol partial pressure (p_M) on the steady state rate of formation of DME over 1.0 g tungstena/zirconia at 127°C, p_{total} = 1360 kPa, and 18.7% N_2/He + alcohol feed rate of 125 mol/kg catalyst/h.

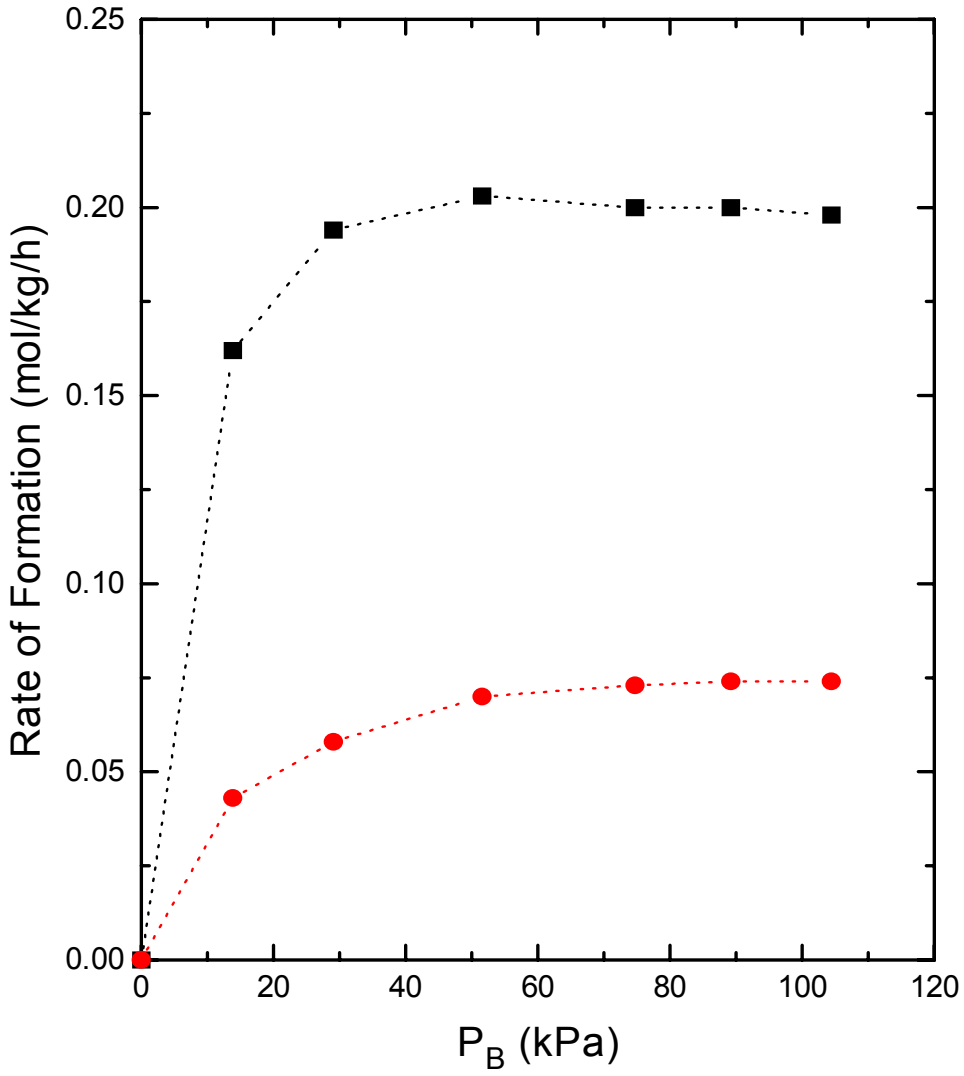

Figure 5. Effect of isobutanol partial pressure (p_B) on the steady state reaction rates for the major products, isobutene ( ) and isooctene ( ), over 1.0 g tungstena/zirconia at 127°C, p_{total} = 1360 kPa, and 18.7% N_2/He + alcohol feed rate of 125 mol/kg catalyst/h.

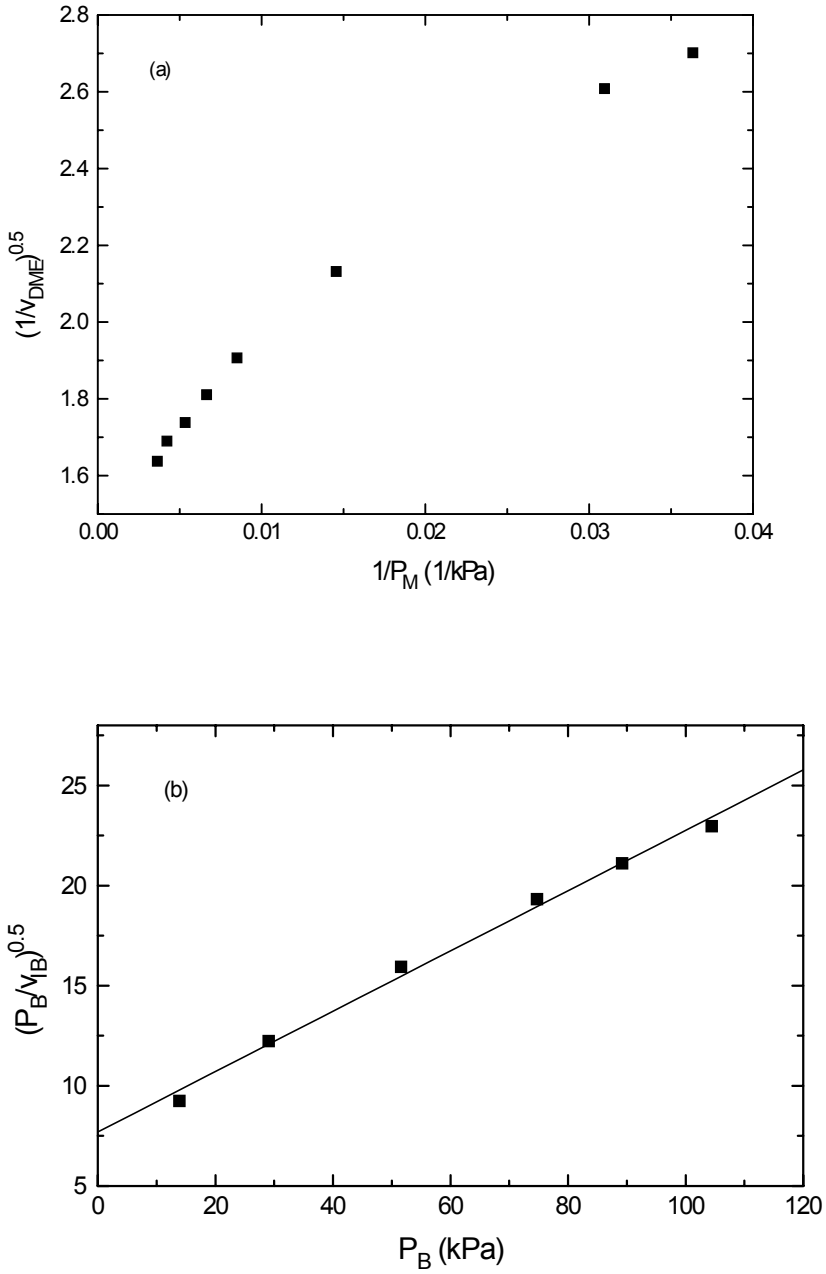

Figure 6. Langmuir-Hinshelwood linear plot for the dehydration of (a) methanol and (b) isobutanol over 1.0 g tungstena/zirconia catalyst at 127°C, p_{total} = 1360 kPa. The slope and intercept give combinations of rate and equilibrium constants (a) 1 / %k_1 = 1.25 for the two highest p_M data points and 2.06 for the two lowest p_M data points and 1 / %k_1K_M = 91.3 and 17.8, respectively, and (b) %(1 / (k_3K_B)) = 7.7 and %(K_B / k_3) = 0.15. k is in units of mol/kg catalyst/h and K_M and K_B are in kPa^{-1}.

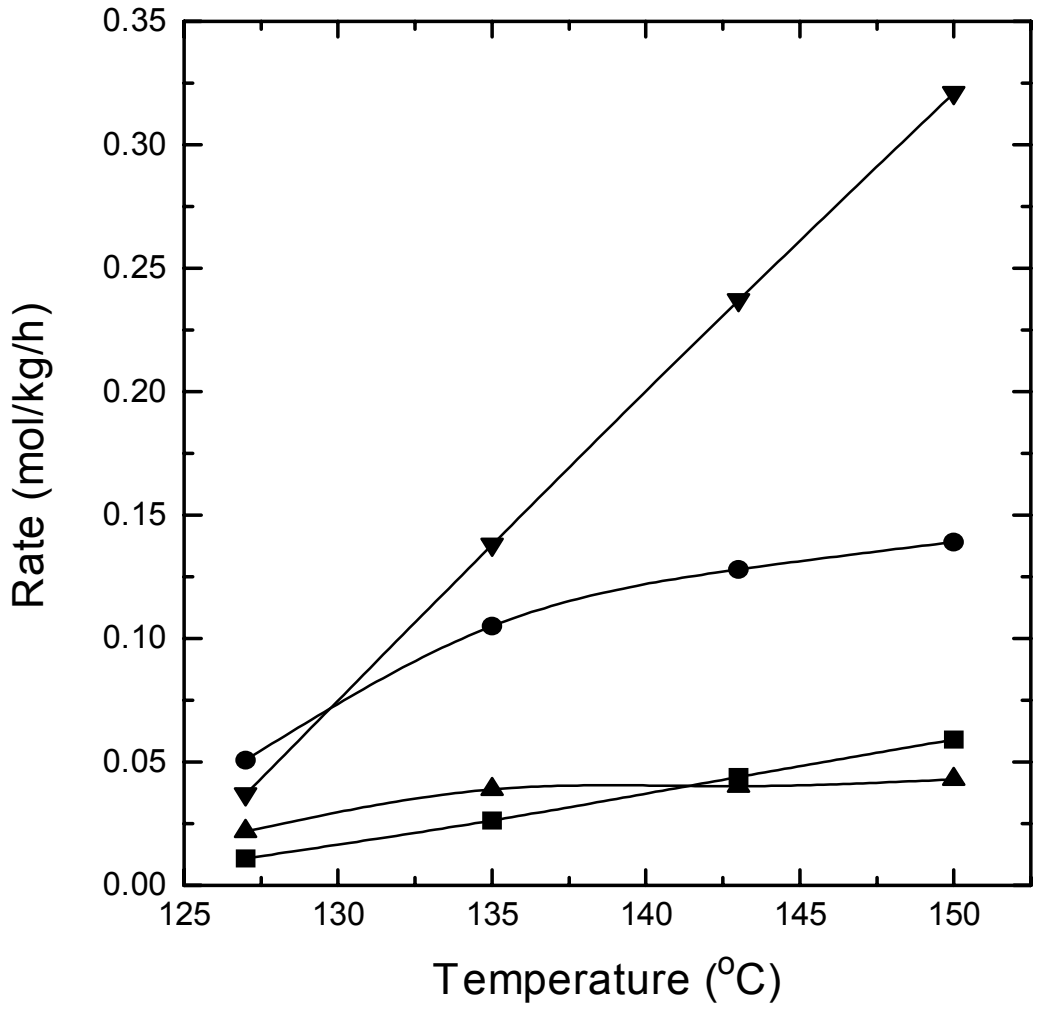

Figure 7. Effect of temperature on the steady state reaction rates of MIBE (C), butenes (?), octene (>), and DME ( ) over 1.0 g tungstena/zirconia with methanol/isobutanol = 2/1 at p_{total} = 1360 kPa, and 18.7% N_2/He + alcohol feed rate of 125 mol/kg catalyst/h.

higher temperatures (>130°C) butenes predominated. The butenes, octenes, and DME were the next in decreasing order. Increasing the reaction temperature resulted in an increase in the formation of all products, but butenes were the dominant product at 135°C and higher temperatures. MIBE became the second most abundant product. MTBE, an isomer of MIBE, was formed in a smaller amount, typically 5% of the amount of MIBE regardless of reaction temperature. Among butenes, isobutene was the major product, while linear butenes formed between 15 and 25% of the amount of isobutene. Thus, the higher the reaction rate, the larger the quantity of linear butenes that were formed. Among the octenes, 2,5-dimethylhexene was predominant over the entire temperature range, with increasing selectivity to 2,2,4-trimethylpentene as temperature increased.

The apparent activation energy for the formation of individual products was determined from Arrhenius plots, as shown in Figure 8. Apparent activation energies were as follows: 113 " 8 kJ/mol for DME, 67 " 17 kJ/mol for MIBE, 121 " 29 kJ/mol for isobutene, and 38 " 17 kJ/mol for isooctene. In the case of gel-type Nafion H at 1344 kPa, the values determined were 84.2-87.5 kJ/mol for DME, 84.3 kJ/mol for MIBE, 144.6 kJ/mol for butenes + octenes [11]. In comparison, with a porous Nafion-H MS catalyst at 7600 kPa, the obtained activation energies were 79 kJ/mol for DME, 61 kJ/mol for MIBE, and 227 kJ/mol for isobutene [24]. The activation energies for ether formation are thus lower than the activation energies for olefin formation on both WZ and Nafion-H catalysts.

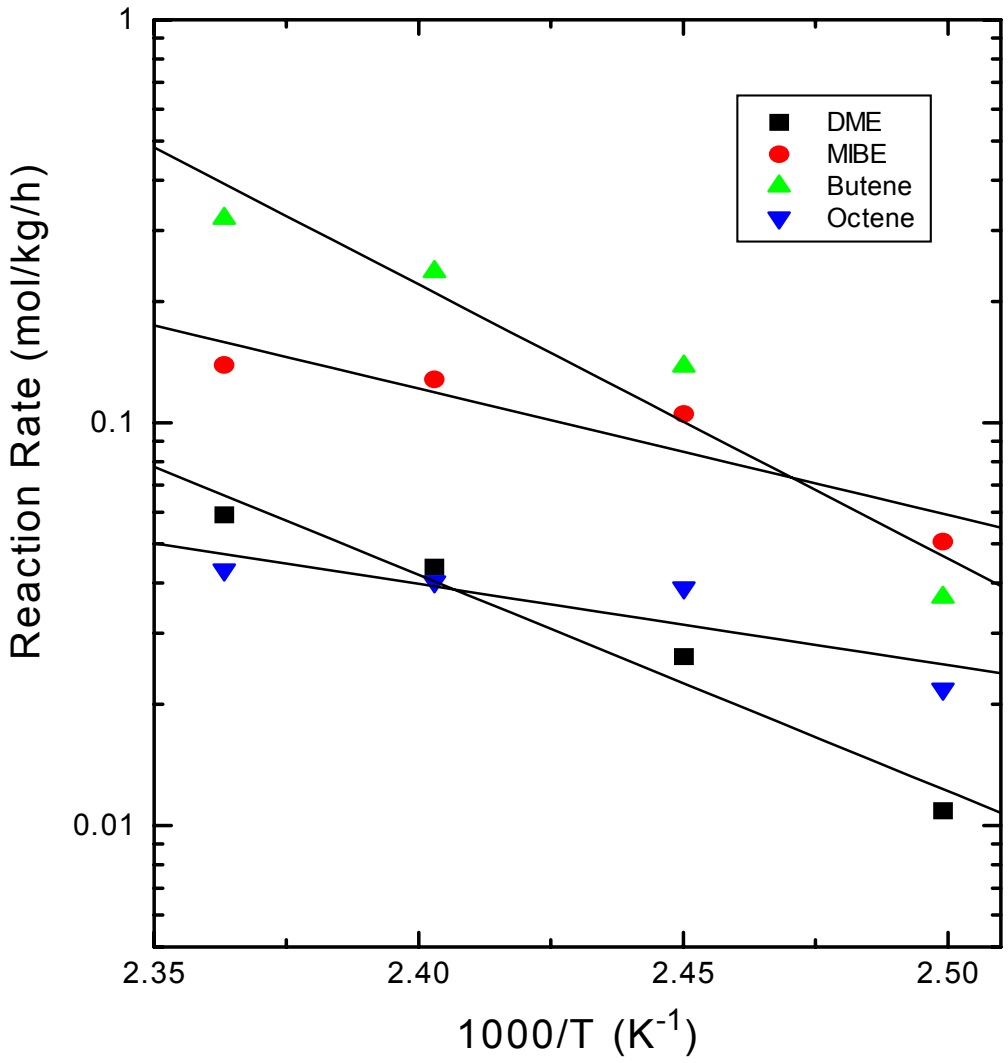

Figure 8. Arrhenius plots of the formation rates of the major products MIBE (C), butenes (?), octenes (>), and DME ( ) formed over the tungstena/zirconia catalyst with methanol/isobutanol = 2/1 at p_{total} = 1360 kPa, and 18.7% N_2/He + alcohol feed rate of 125 mol/kg catalyst/h.

OPTICAL PROPORTIES OF THE CATALYSTS

Diffuse reflectance studies were carried out in the ultraviolet/visible/near-infrared (UV/Vis/NIR) spectral regions to provide information on the electronic structure, the degree of hydration, and presence of hydroxyl groups of zirconia, tungstena/zirconia, and sulfated zirconia samples.

Spectral Data and Analysis. The optical spectra of the three dehydrated samples were collected over the range of 4,500-50,000 cm^{-1}. The diffuse reflectance spectra (DRS) over this full spectral range are shown in Figure 9. It is clear that the optical properties of the three samples reflect the structure and composition of the catalysts.

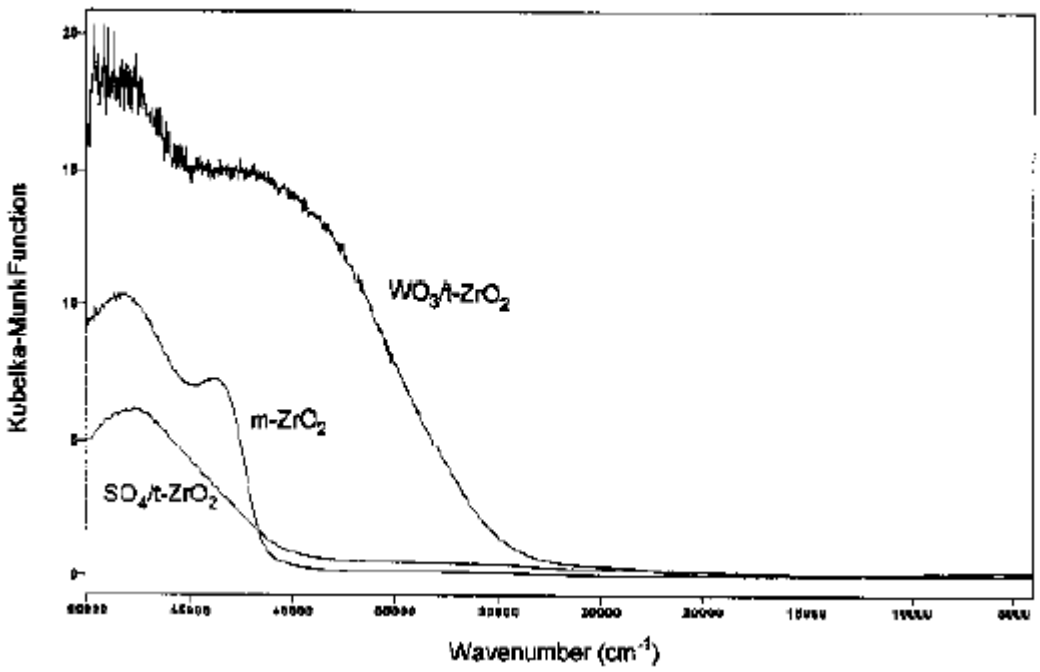

Figure 9. The diffuse reflectance spectra of monoclinic zirconia (m-ZrO_2), tetragonal SO_4-impregnated zirconia (SO_4/t-ZrO_2), and tetragonal WO_3-impregnated zirconia (WO_3/t-ZrO_2) between 4,500 and 50,000 cm^{-1}.

The spectra in the NIR region are shown in Figure 10. For the three samples, the two particular bands of interest in the NIR region are the H_2O (v + *) band at about 5,250 cm^{-1}, which is a combination of stretching and bending modes, and the mixed H_2O (2v) + OH (2v) overtone band of the OH stretch at approximately 7,200 cm^{-1}. The former can be used to monitor the degree of dehydration, while the latter can be used to monitor the hydroxyl groups, which are Brønsted acid sites. These groups are present on ZrO_2. Upon sulfating the zirconia, a larger peak at 7159 cm^{-1} was observed, corresponding to an increased number of hydroxyl groups (Brønsted acid sites). Upon tungstating the zirconia, a high optical background was observed and the number of free hydroxyls detected greatly decreased, as indicated by the low intensity of the 7092 cm^{-1} band compared with the ZrO_2 bands.

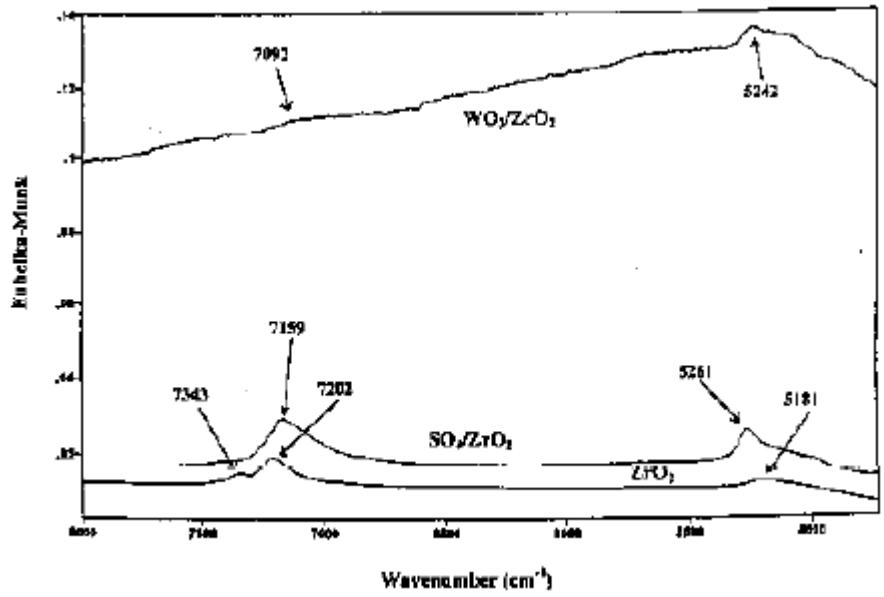

Figure 10. DRS in the NIR region of monoclinic zirconia, tetragonal SO_4-impregnated zirconia, and tetragonal WO_3-impregnated zirconia in the spectral range of 4,500 and 8,000 cm^{-1}. Peak positions are labelled, but accurate calibration needs to be carried out.

The difference spectrum in the OH NIR region of the WO_3/ZrO_2 catalyst was derived for comparison with the distinct spectrum of ZrO_2 that exhibits two peaks. The absorption spectrum for WO_3/ZrO_2 is shown on the same scale as for ZrO_2 in Figure 11. Also shown is the difference spectrum for WO_3/ZrO_2 that was obtained by magnifying the Kubelka-Munk transformed spectra by a factor of 10 and subtracting the background. The diminished intensity of the OH frequencies upon surface impregnation of the zirconia with tungstate indicates bonding of the tungstate species to the surface of the zirconia *via* the surface hydroxyl groups and that it is spread on the surface. There are relatively few hydroxyls present on the tungstated zirconia surface, and those exhibit a shift from . 7205 cm^{-1} on monoclinic zirconia to *ca.* 7120 cm^{-1} on the tungstated zirconia surface, perhaps arising from low-concentration Brønsted acid sites on the tungstate overlayer.

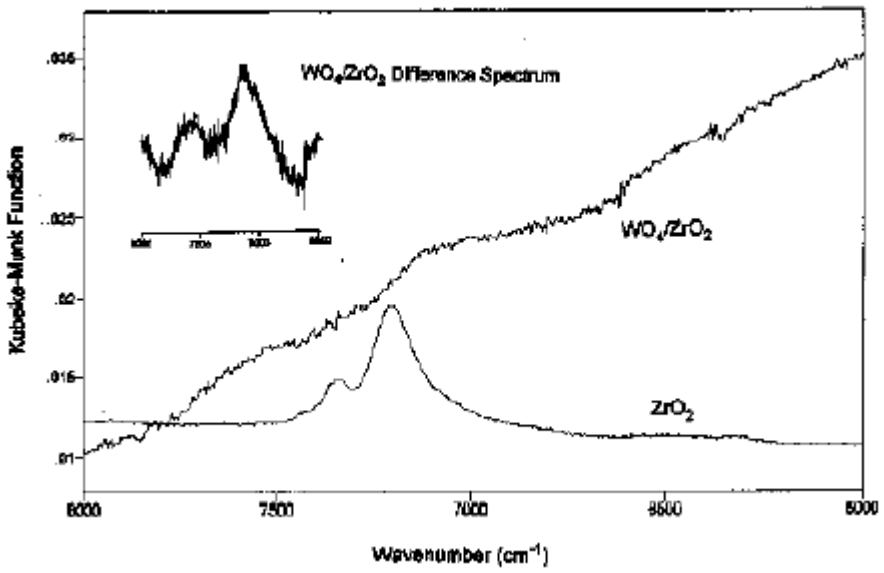

FIGURE 11. The NIR-DRS spectra of the hydroxyl absorption region for monoclinic zirconia and tetragonal tungstated zirconia on the same relative scale, along with the magnified difference spectrum obtained for the latter sample.

The areas of the two bands in the NIR region at about 5,250 cm^{-1} [H_2O (v + *) combination band] and at approximately 7,200 cm^{-1} [mixed H_2O (2v) + OH (2v) overtone band] were calculated for each sample by subtracting a linear background and fitting multiple (usually 3-5) Gaussians to the bands. The areas of the Gaussians in the peak were then summed, and the results of the Gaussian fitting are shown in Table 1.

The approximate concentrations of hydroxyls on the three samples were then calculated based on the assumption that the relative intensities of the H_2O (v + *) and H_2O (2v) bands were in the ratio of 5/1, as in earlier studies [25]. The equation, derived from this work, to calculate the intensity of the OH (2v) band from the intensities of the mixed H_2O (2v) + OH (2v) overtone band and the H_2O (v + *) combination band is

$$\mathbf{I}_{[H2O\ (2v) + OH\ (2v)\ mixed\ band]} = \mathbf{I}_{OH\ (2v)} + [\mathbf{I}_{H2O\ (v + *)} / 5], \qquad (8)$$

where **I** = the integrated intensity or peak area.

The hydroxyl concentration of the tetragonal zirconia impregnated with surface sulfate was determined in this laboratory [23] using a method of controlled incremental adsorption and desorption of different nitrogen-containing bases. The surface sulfate concentration was found to be 0.55 monolayer. The concentrations of hydroxyls on the tetragonal WO_3-impregnated zirconia and on monoclinic zirconia were calculated by using the known hydroxyl concentration of the tetragonal SO_4-impregnated zirconia, calculated as $\mathbf{I}_{OH\ (2v)}$ intensities, and Equation 8 given above. The calculated hydroxyl concentrations are given in Table 2. In all cases, the OH surface concentration was determined to be appreciably less than one monolayer.

Table 1. The Gaussian fitting results of the H_2O (v + *) combination bands and the mixed H_2O (2v) + OH (2v) overtone bands in the NIR regions of monoclinic zirconia, tetragonal SO_4-impregnated zirconia, and tetragonal WO_3-impregnated zirconia as determined by DRS.

Sample	2v Bands (H_2O and OH)			H_2O (v + *) Bands		
m-ZrO_2	No. of Gaussian Peaks In Band			No. of Gaussian Peaks In Band		
	Peak	Peak Center	Peak Area	Peak	Peak Center	Peak Area
	1	7424.095	0.0473	1	5364.610	0.0304
	2	7144.920	0.6076	2	5301.622	0.0278
	3	7348.438	0.1703	3	5228.950	0.1210
	4	7208.340	0.6081	4	5158.892	0.0193
	--			5	5129.900	0.2517
	Total Peak Area: 1.4332			Total Peak Area: 0.4502		
WO_3/ t-ZrO_2	No. of Gaussian Peaks In Band			No. of Gaussian Peaks In Band		
	Peak	Peak Center	Peak Area	Peak	Peak Center	Peak Area
	1	7612.789	0.2289	1	5077.164	0.1458
	2	7508.370	0.0415	2	5155.256	0.4088
	3	7369.754	0.0699	3	5244.010	0.4266
	4	7124.459	0.3093	--		
	5	6987.467	0.1835	--		
	6	6842.649	0.1093	--		
	Total Peak Area: 0.9423			Total Peak Area: 0.9812		

Sample	2v Bands (H_2O and OH)			H_2O (v + *) Bands		
	No. of Gaussian Peaks In Band			No. of Gaussian Peaks In Band		
	Peak	Peak Center	Peak Area	Peak	Peak Center	Peak Area
	1	7147.057	0.5412	1	5354.494	0.0060
	2	7116.763	1.9706	2	5264.007	0.4595
	--			3	5197.272	0.0426
	--			4	5181.609	0.7589
SO_4/ t-ZrO_2	Total Peak Area: 2.5118			Total Peak Area: 1.2670		

TABLE 2. The hydroxyl concentrations calculated from the diffuse reflectance spectra, given in monolayers, of monoclinic zirconia, tetragonal WO_3-impregnated zirconia, and tetragonal SO_4-impregnated zirconia.

Sample	$\mathbf{I}_{OH\ (2v)}$	OH Conc. (monolayers)
ZrO_2	0.74607	0.18
WO_3/ZrO_2	1.34345	0.33
SO_4/ZrO_2	2.25835	0.55

Conclusions from Optical Spectroscopy. The samples have well-developed band edges, especially for the monoclinic ZrO_2 with a band edge at about 42,000 cm^{-1}. For the tetragonal SO_4/ZrO_2 catalyst, the band edge is shifted to the UV region (. 45,000 cm^{-1}), while for the tetragonal WO_3/ZrO_2 catalyst, the band edge is shifted toward the visible (VIS) region (. 35,000 cm^{-1}) and has a very large intensity with an extended tailing. The spectra can be used for diagnostics/quality control of preparation, in combination with XRD.

The NIR peaks in the 5,000-5,500 cm^{-1} region confirm the presence of water in these samples. Assignment of the NIR bands is difficult when a sample is not fully dehydrated, but the spectral shoulders below the peaks at 7159 and 7202 cm^{-1} in the tetragonal SO_4/ZrO_2 and monoclinic ZrO_2, respectively, are indicative of weakly bonded hydroxyls. A very slight shoulder is barely detectable on the peak at 7092 cm^{-1} in the tetragonal WO_3/ZrO_2 spectrum, suggesting that this sample was only partially hydroxylated.

The NIR spectra give information about sample hydroxylation. It is shown that ZrO_2 has a low degree of hydroxylation (. 18%) and has little water of hydration associated with it. The hydroxyl concentration of the tetragonal SO_4/ZrO_2 catalyst was determined earlier [23] and can be used as a "benchmark". The tetragonal WO_3/ZrO_2 catalyst has weak and broad features in the hydroxyl region of the spectrum and is difficult to analyze. However, it is clear that this catalyst is less hydroxylated than the SO_4/ZrO_2 catalyst. It is noted that the WO_3/ZrO_2 catalyst has a larger electronic background in the NIR region than the other two catalysts. Quantitative analysis of the hydroxyl species in these catalysts has been carried out, but more calibration studies with reference systems are needed to achieve greater accuracy.

The UV regions of the spectra reflect electronic band-to-band transitions and show significant differences among the samples. Strong bands in the 35,000 to 48,000 cm^{-1} spectral range are observed. The spectral inflection point of tetragonal SO_4/ZrO_2 occurs at 45,000 cm^{-1}. The inflection points of the band edges of monoclinic ZrO_2 and tetragonal WO_3/ZrO_2 samples occur at about 42,225 and 34,300 cm^{-1}, respectively. In addition, the tetragonal WO_3/ZrO_2 sample shows a weak band near 25,000 cm^{-1}, while the monoclinic

ZrO_2 shows a very weak band near 32,500 cm^{-1}. These transitions giving rise to these bands can be interpreted theoretically based on electronic structure.

XPS STUDIES OF THE ACIDITY OF WO_3/ZrO_2

This study is focusing on the diagnostics of surface acid sites to provide insight into catalyst optimization for coupling alcohols to ethers. The solid acid centers were subjected to quantitative analysis of their concentration and strength by X-ray photoelectron spectroscopy using amines as adsorbing probe molecules. The core-level N 1s photoemission exhibits a large shift towards higher binding energies upon protonation, which occurs upon interaction with Brønsted acid sites. This has been demonstrated with pyridine adsorption on Nafion-H, where the Brønsted acid sites gave rise to a N 1s peak at 401.6 eV compared with physisorbed pyridine at 398.8 eV [23]. Similarly, adsorption of pyridine on sulfated zirconia gave rise to N 1s binding energy peaks at 399.3-399.9 eV and at 401.5 eV, which were attributed to adsorption of pyridine on Lewis and Brønsted acid sites, respectively [23]. Thus, Lewis and Brønsted acid sites can be distinguished and quantified on solid acid catalysts.

For the present studies, the amines chosen were pyridine (a weak base), triethylamine (TEA, a strong base), and ethylenediamine (EDA, a bifunctional base). Survey and high resolution XPS spectral scans of the catalysts were taken before and after amine adsorption. For the zirconia samples, high resolution scans of Zr 3d, C 1s, W 4f, and N 1s regions were carried out. The $3d_{5/2}$ Zr core-level peak for clean WO_3/ZrO_2 was chosen as the reference peak for binding energy position.

A survey spectrum of the W/Z catalyst is shown in Figure 12. High resolution scans of the W 4f and Zr 3d peaks were obtained, and the observed binding energies (B.E.) and peak intensities for Zr and W are shown in Table 3 for the "clean" W/Z catalyst prior to adsorption of an amine, where FWHM is the full width at half-maximum of the peak. The peak areas were obtained by first curve-fitting the spectra using a computer program supplied with the Scienta instrument. The spectra were fitted to a Voigt function using at least 10 iterations to obtain a good fit, as defined by a "goodness-of-fit" factor based on the number of data points utilized [23]. The sensitivity factors correspond to the photoelectron cross sections that are based on theoretical calculations by Scofield [26], as tabulated in the Scienta software, but some have been refined in this laboratory by numerous practical measurements [23]. For example, the Scofield cross section for O 1s was given as 2.93, while a sensitivity factor for O 1s of 2.837 was utilized in this work. Similarly, the Scofield cross section given for N 1s was 1.80, while the sensitivity factor used in the present work was 1.62.

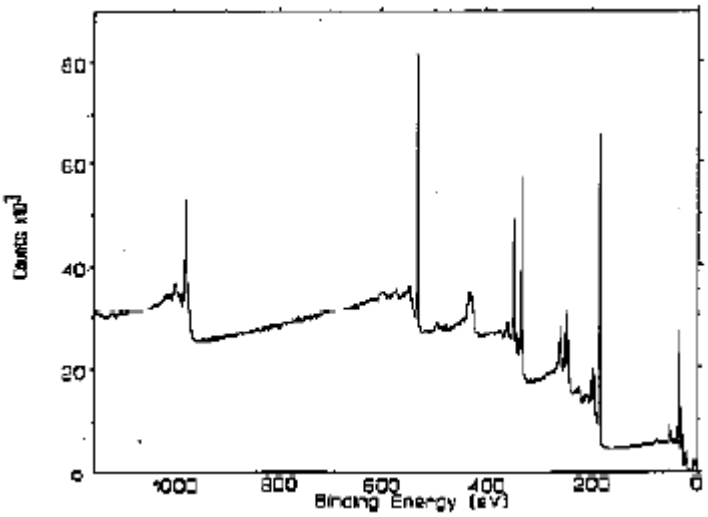

FIGURE 12. XPS survey spectrum of the W/Z catalyst.

TABLE 3. Binding energies and intensities observed for the Zr and W XPS peaks for the clean W/Z catalyst.

Peak	B.E. (eV)	FWHM (eV)	Peak Area	Sensitivity Factor	Peak Intensity
Zr $3d_{total}$	---	---	1.598×10^4	7.04	2.270×10^3
Zr $3d_{5/2}$	182.19	1.56	9.506×10^3	4.17	2.280×10^3
W $4f_{total}$	---	---	3.722×10^3	9.80	3.798×10^2
W $4f_{5/2}$	37.57	1.47	1.637×10^3	4.32	3.789×10^2
W $4f_{7/2}$	35.45	1.55	2.079×10^3	5.48	3.794×10^2

After adsorption of pyridine onto the W/Z catalyst using the procedure described in the Experimental section of this report, the N 1s spectral region was scanned, and the spectrum was resolved into two peaks, as shown in Figure 13. The observed binding energies and peak intensities are given in Table 4. The pyridine adsorption indicated that most of the titrated acid sites were Brønsted acid sites, where the adsorbed pyridine had the N 1s binding energy of 401.64 eV. The presence of a N 1s peak located at lower binding energy was also indicated in the spectrum.

Similar experiments were carried out using ethylenediamine (EDA) as the adsorbing base. The resultant N 1s spectrum is shown in Figure 14. The analysis of the XPS spectral data is compiled in Table 5. It was observed that the two N 1s peaks exhibited similar intensities, indicating the presence of two N species that were approximately equal in number.

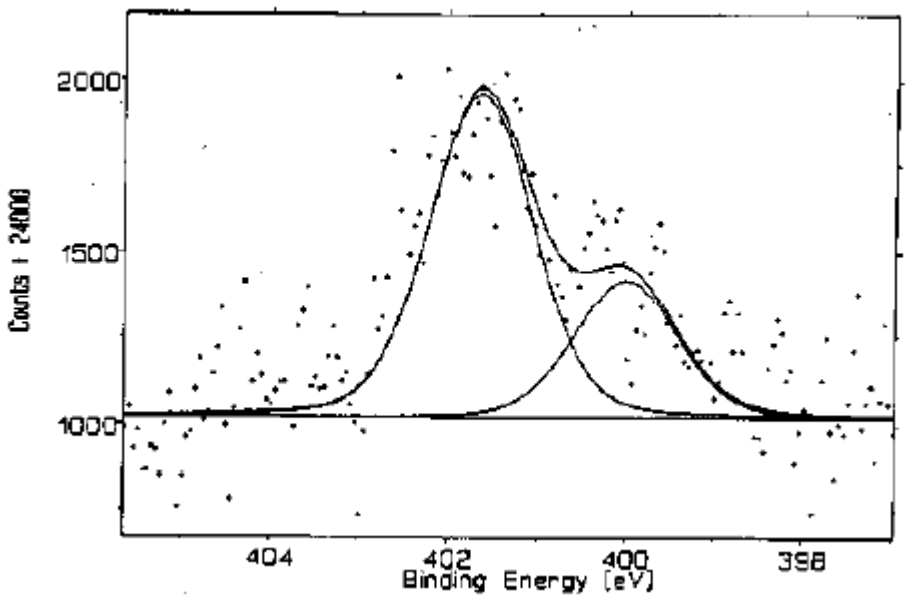

FIGURE 13. XPS spectrum of the N 1s peak for the W/Z catalyst after evacuation at 150EC, adsorption of pyridine at ambient temperature, and evacuation at 150EC. The resolved peaks (solid lines) are fitted to the experimental data points.

TABLE 4. Binding energies and intensities observed for the Zr and W peaks for the W/Z catalyst after evacuation at 150EC, adsorption of pyridine at ambient temperature, and evacuation at 150EC.

Peak	B.E. (eV)	FWHM (eV)	Peak Area	Sensitivity Factor	Peak Intensity
Zr $3d_{total}$	---	---	1.340×10^4	7.04	1.903×10^3
Zr $3d_{5/2}$	182.19	1.38	7.931×10^3	4.17	1.902×10^3
W $4f_{total}$	---	---	3.834×10^3	9.80	3.912×10^2
W $4f_{5/2}$	37.57	1.36	1.691×10^3	4.32	3.914×10^2
W $4f_{7/2}$	35.45	1.47	2.147×10^3	5.48	3.918×10^2
N $1s_{total}$	---	---	1.425×10^2	1.62	8.796×10^1
N $1s_B$	401.64	1.35	9.056×10^1	1.62	5.590×10^1
N $1s_L$	400.01	1.35	3.842×10^1	1.62	2.372×10^1

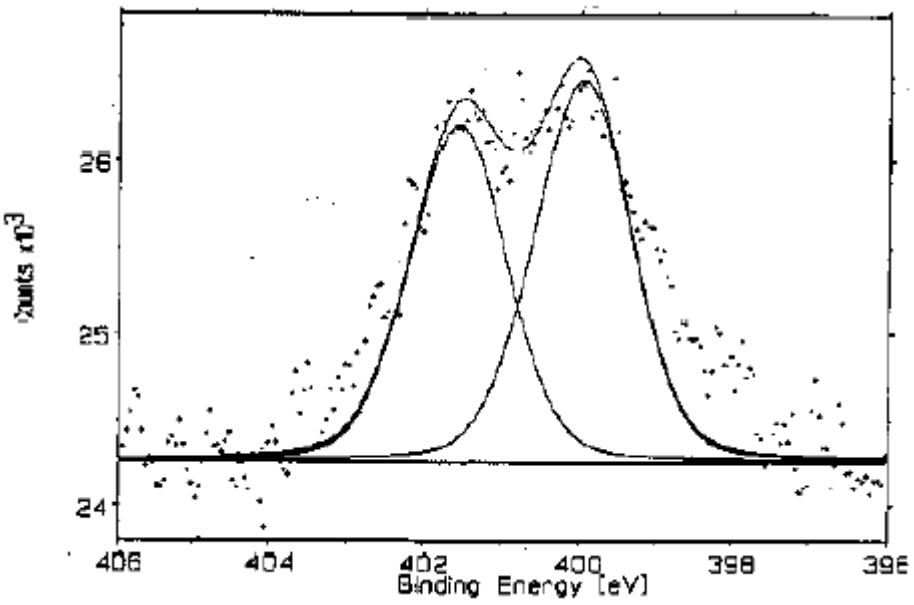

FIGURE 14. XPS spectrum of the N 1s peak for the W/Z catalyst after evacuation at 150EC, adsorption of ethylenediamine at ambient temperature, and evacuation at 150EC.

TABLE 5. Binding energies and intensities observed for the Zr and W peaks for the W/Z catalyst after evacuation at 150EC, adsorption of ethylenediamine (EDA) at ambient temperature, and evacuation at 150EC.

Peak	B.E. (eV)	FWHM (eV)	Peak Area	Sensitivity Factor	Peak Intensity
Zr $3d_{total}$	---	---	1.310×10^4	7.04	1.861×10^3
Zr $3d_{5/2}$	182.18	1.45	7.765×10^4	4.17	1.862×10^3
W $4f_{total}$	---	---	3.499×10^3	9.80	3.570×10^2
W $4f_{5/2}$	37.56	1.38	1.540×10^3	4.32	3.567×10^2
W $4f_{7/2}$	35.42	1.47	1.958×10^3	5.48	3.573×10^2
N $1s_{total}$	---	---	4.917×10^2	1.62	3.035×10^2
N $1s_B$	401.57	1.45	2.022×10^2	1.62	1.248×10^2
N $1s_L$	399.97	1.45	2.286×10^2	1.62	1.411×10^2

Similarly, triethylamine (TEA) was utilized as the absorbing nitrogen-containing base to probe the surface acid sites. The observed N 1s XPS spectrum is shown in Figure 15. Again, the spectrum was adequately fitted by two peaks. The XPS data of TEA on the W/Z catalyst are summarized in Table 6.

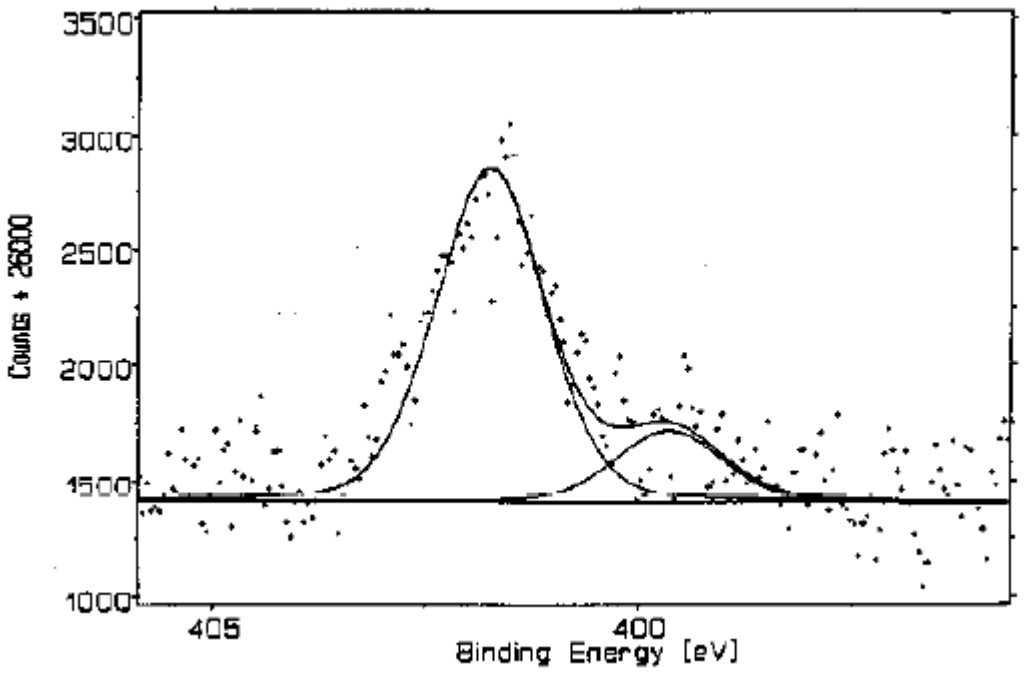

FIGURE 15. XPS spectrum of the N 1s peak for the W/Z catalyst after evacuation at 150EC, adsorption of triethylamine (TEA) at ambient temperature, and evacuation at 150EC.

TABLE 6. Binding energies and intensities observed for the Zr and W peaks for the W/Z catalyst after evacuation at 150EC, adsorption of triethylamine (TEA) at ambient temperature, and evacuation at 150EC.

Peak	B.E. (eV)	FWHM (eV)	Peak Area	Sensitivity Factor	Peak Intensity
Zr $3d_{total}$	---	---	1.511×10^4	7.04	2.146×10^3
Zr $3d_{5/2}$	182.22	1.31	8.951×10^3	4.17	2.146×10^3
W $4f_{total}$	---	---	4.370×10^3	9.80	4.459×10^2
W $4f_{5/2}$	37.66	1.31	1.930×10^3	4.32	4.467×10^2
W $4f_{7/2}$	35.51	1.28	2.450×10^3	5.48	4.471×10^2
N $1s_{total}$	---	---	2.104×10^2	1.62	1.298×10^2
N $1s_B$	401.74	1.50	1.527×10^2	1.62	9.426×10^1
N $1s_L$	399.64	1.50	3.310×10^1	1.62	2.043×10^1

PART II: STUDIES OF THE ETHER SYNTHESIS NAFION-H CATALYST

XPS STUDIES OF THE ACIDITY OF THE NAFION-H CATALYST

The **Nafion-H microsaddles** (MS) resin catalyst was also characterized by XPS analysis. Nafion-H is a fluorocarbon copolymer containing sulfonyl groups that is an insulating material and suffered charging. Therefore, a hot filament flood gun was utilized to neutralize the charging. In addition, the measured binding energies for Nafion-H samples were adjusted using the C 1s line for poly(tetrafluoroethylene) (PTFE) at 292.48 eV [27] as an internal standard. The F 1s peak for PTFE was observed at 689.67 eV [27].

The data for a clean evacuated Nafion-H MS sample are given in Table 7. Two O 1s binding energy peaks are noted. The higher binding energy peak (535.84 eV) is due to oxygen in ether linkages in the polymer backbone of the resin, while the peak at 533.31 eV corresponds to the oxygen associated with the sulfonic acid groups [20,27]. This is consistent with an O/S ratio = 3 for the sulfonic group, i.e. $!CF_2SO_3H$, where the experimental ratio from Table 7 is 2.9.

TABLE 7. Binding energies and intensities observed for the clean Nafion-H MicroSaddles (MS) catalyst after evacuation.

Peak	B.E. (eV)	FWHM (eV)	Peak Area	Sensitivity Factor	Peak Intensity
F 1s	689.72	2.04	3.811×10^4	4.5880	8.306×10^3
S 2p	---	---	9.503×10^2	2.1735	4.372×10^2
$S\ 2p_{1/2}$	171.60	1.68	3.166×10^2	0.7245	4.370×10^2
$S\ 2p_{3/2}$	170.27	1.68	6.333×10^2	1.4490	4.371×10^2
$C\ 1s_{total}$	---	---	4.725×10^3	1	4.725×10^3
	294.12	1.70	8.826×10^2	1	8.826×10^2
	292.47	1.45	3.646×10^3	1	3.646×10^3
O 1s	535.84	2.50	1.970×10^3	2.837	6.944×10^2
	533.31	1.84	3.609×10^3	2.837	1.272×10^3

After evacuation of the Nafion-H MS sample, equilibration with ethylenediamine (EDA) was carried out, and then XPS spectra were obtained after evacuation but without heat treatment of the sample. The resultant N 1s spectrum is shown in Figure 16. The peak is slightly asymmetric, and it was fitted by two Gaussians of equal intensity. The N 1s XPS data resolved for two peaks are given in Table 8.

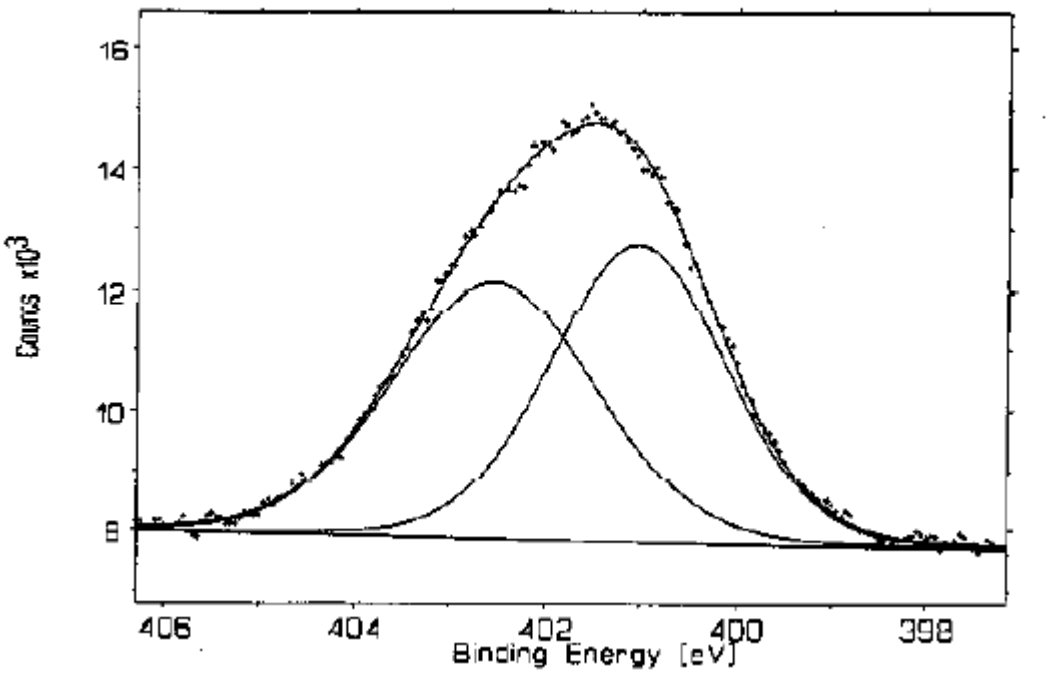

FIGURE 16. XPS N 1s spectrum of Nafion-H MS after adsorption of ethylenediamine (EDA), with no thermal post-treatment.

TABLE 8. Binding energies and intensities observed for the Nafion-H MS catalyst after adsorption of ethylenediamine (EDA), with no thermal post-treatment.

Peak	B.E. (eV)	FWHM (eV)	Peak Area	Sensitivity Factor	Peak Intensity
F 1s	689.76	2.06	4.224×10^4	4.5880	9.206×10^3
S 2p	---	---	3.379×10^2	2.1735	1.555×10^2
S $2p_{1/2}$	171.46	2.64	1.120×10^2	0.7245	1.546×10^2
S $2p_{3/2}$	170.09	2.36	2.240×10^2	1.4490	1.546×10^2
C $1s_{total}$	---	---	5.347×10^3	1	5.347×10^3
	294.09	1.82	1.360×10^3	1	1.360×10^3
	292.47	1.44	3.832×10^3	1	3.832×10^3
O 1s	536.27	2.21	1.904×10^3	2.837	6.711×10^2
	533.21	2.08	1.966×10^3	2.837	6.930×10^2
N $1s_{total}$	---	---	1.317×10^3	1.62	8.130×10^2
	402.55	2.51	6.584×10^2	1.62	4.064×10^2
	401.03	2.16	6.584×10^2	1.62	4.064×10^2

The Nafion-H MS sample with the adsorbed ethylenediamine (EDA) was subsequently evaculated while being heated at 150EC. The sample was then analyzed again by XPS at ambient temperature, and the resultant N 1s spectrum is shown in Figure 17. The top of the peak appears to be flatter, and the peak can again be resolved into two peaks of equal intensity. The analysis of the XPS data is tabulated in Table 9.

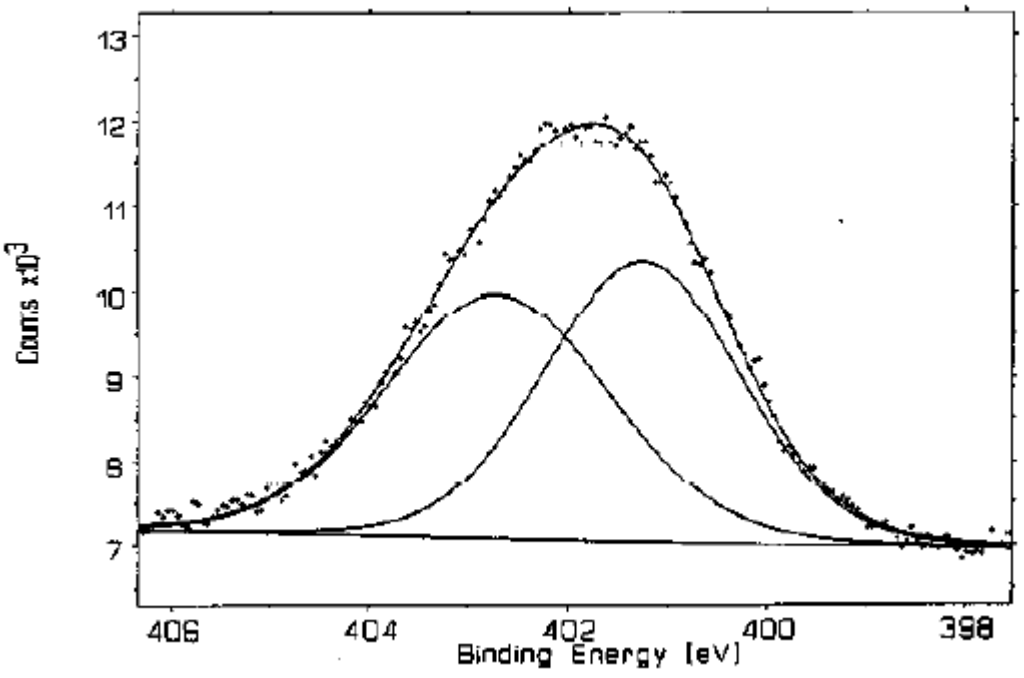

FIGURE 17. XPS N 1s spectrum of Nafion-H MS after adsorption of ethylenediamine (EDA), followed by a thermal post-treatment at 150EC.

As shown, the titration of acid sites gives different results with the different amines. Pyridine titrates 13% of the Brønsted acid sites, while TEA, a strong base that could be sterically hindered on the surface, titrates 22% of the acid sites. EDA titrates 37% of the Brønsted acid sites. Therefore, the accessibility of the Brønsted acid sites on W/Z follows the order of EDA > TEA > pyridine, while the basicity of the amines follows the order TEA > EDA > pyridine. The tungstated zirconia is not the same as the sulfated zirconia (S/Z). With the latter catalyst, pyridine titrates all Brønsted acid sites, while that is not the case with the tungstated zirconia.

TABLE 9. Binding energies and intensities observed for the Nafion-H MS catalyst after adsorption of ethylenediamine (EDA), followed by thermal post-treatment of evacuation at 150EC.

Peak	B.E. (eV)	FWHM (eV)	Peak Area	Sensitivity Factor	Peak Intensity
F 1s	689.74	2.16	4.265×10^4	4.5880	9.296×10^3
S 2p	---	---	2.709×10^2	2.1735	1.206×10^2
S $2p_{1/2}$	171.75	2.64	9.046×10^1	0.7245	1.249×10^2
S $2p_{3/2}$	170.26	2.36	1.809×10^2	1.4490	1.248×10^2
C $1s_{total}$	---	---	5.581×10^3	1	5.581×10^3
	294.09	1.82	1.716×10^3	1	1.716×10^3
	292.47	1.44	3.693×10^3	1	3.693×10^3
O 1s	536.22	2.21	2.008×10^3	2.837	7.078×10^2
	533.26	2.08	1.496×10^3	2.837	5.273×10^2
N $1s_{total}$	---	---	9.404×10^2	1.62	5.805×10^2
	402.71	2.51	4.701×10^2	1.62	2.902×10^2
	401.26	2.16	4.701×10^2	1.62	2.902×10^2

It is concluded from this study that the amine bases titrate the Brønsted acid sites on these acid catalysts. However, the surface concentration of the accessible acid sites on the tungstena/zirconia catalyst is lower than expected from the tungstate content and are more diluted than observed with the Nafion-H catalyst. In addition, the Brønsted acid sites on the tungstena/zirconia catalyst are heterogeneous since stronger amine bases detect more acid sites.

MODELLING OF ETHER SYNTHESIS OVER NAFION-H

Kinetic results suggest that the mechanism of the ether-forming reaction on WZ is the same as on SZ and Nafion-H. We are examining the dual-site S_N2 reaction pathway theoretically *via ab initio* DFT (BP86, DN**) calculations [28] of the prototype system 2S + M + B (S / CF_3SO_3H, M / CH_3OH, B / $(CH_3)_2CHCH_2OH$). These computations are being extended to DME synthesis for comparison.

Geometries have been optimized and true global minima have been found. The transition state (TS) has been found that satisfies the criteria of one imaginary frequency with root mean square gradient of 0.00023 hartree/D. The calculated total energies are) E(S) = !962.4218,) E(M) = !115.7793, and) E(B) = !194.4431 hartrees, respectively, and energy differences on the reaction pathway are given in Table 10.

The calculated energies for MIBE synthesis are shown in Table 10, and the results demonstrate that:

(1) the TS barrier from free reactants, $E^{\ddagger}$ – 16 kcal/mol, is comparable to the experimental 15 kcal/mol obtained with Nafion-H [12,24],

(2) the overall reaction is nearly thermally neutral ($E_{(reaction)}$ – !6 kcal/mol), in agreement with thermochemical data ( ) H = !5.53 kcal/mol) [24],

(3) sorbed intermediates involve hydrogen-bonded methanol and more strongly held hydrogen-bonded isobutanol, in agreement with the pattern derived from kinetic data [12],

(4) MIBE is more weakly bonded than the precursor alcohols but H_2O is more strongly

held, and

(5) weak (. 4 kcal/mol) cooperative complex formation between the sorbed methanol and isobutanol reactants or the sorbed products is predicted.

Table 10. Energetics of the dual-site S_N2 pathway M + B ° TS ° MIBE + W over sulfonic acid sites.[a]

1	2		3	4	5	6		7
	2a	2b				6a	6b	
M + B + 2S	M | S	B | S	M@@@@@B ! ! S@@@@@S	TS	MIBE@@@@W ! ! S@@@@@@@S	MIBE ! S	W ! S	MIBE + W + 2S
0	! 14.81	! 13.68	! 22.44	! 6.63	! 28.58	! 12.53	! 10.92	! 1.44

[a]All energies are in kcal/mol, DFT (BP86, DN**) optimized. M / CH_3OH, B / $(CH_3)_2CHCH_2OH$, MIBE / $(CH_3)_2CHCH_2OCH_3$, W / H_2O, S / CF_3SO_3H, and TS / the transition state. The columns represent:

1. Separated alcohol reactants and two acid sites;
2. Alcohols adsorbed on two separate acid sites;
3. Sorbed precursor complex of alcohols and two proximal acid sites;
4. Transition state;
5. Sorbed complex of product MIBE and water on two proximal acid sites;
6. MIBE and water adsorbed on two separate acid sites; and
7. Separated products and two acid sites.

The above features, in conjunction with experimental results, suggest a pathway in which the alcohols are brought together by hydrogen bonding to the proximal sites and the sorption complexes are transformed into the TS by a concerted methyl transfer between the two alcohol oxygens and three protons transfer among the methanol and two sulfonic groups.

The TS structure is shown in Figure 18 with two pathway-driving orbitals involving the carbon C_o of the CH_3 group of MeOH. The i-BuO(H)@@@@CH_3@@@@OH_2 angle is 175.3E and

the CH_3 group is planar as the configuration of the H atoms is being inverted from that in MeOH to that in MIBE. The F-TS orbital (Figure 18A; !32.33 hartree) connects the two Os adjacent to CH_3 as O 2pF-C 2s-O 2pF, and the B-TS orbital (Figure 18B; !18.56 hartree) as O 2pB-C 2pB-O 2pB in an antarafacial fashion. These orbitals are nearly symmetric and are very sensitive to the movement of the CH_3 toward one O or another, tantamount to breaking one C!O bond and strengthening the other.

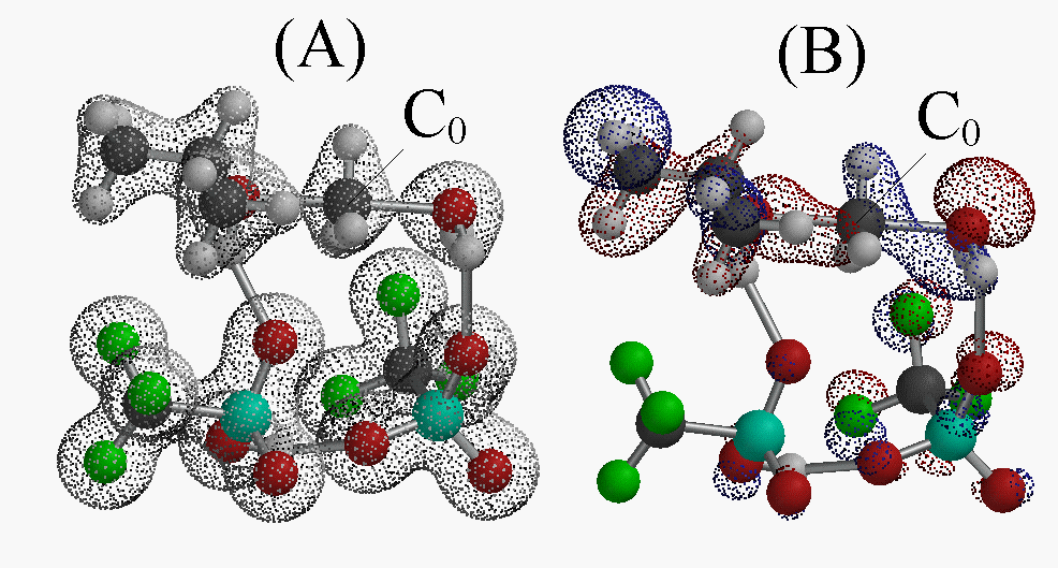

Figure 18. The dual site TS structure for the MeOH + i-BuOH º MIBE + H_2O reaction pathway showing **(A)** the F-TS orbital and **(B)** the B-TS orbital as the methyl group of MeOH moves toward forming the ether linkage. The atoms represented by colors are: red for O, gray for H, black for C, green for F, and blue for S.

Sulfated zirconia and tungstated zirconia have been established as very strong acids [19,23], as have the fluorocarbon sulfonic acids [15,24]. Furthermore, evidence based on hydrocarbon isomerizations indicates that WO_3/ZrO_2 possesses stronger acid sites than SO_4/ZrO_2 [19]. We have herein quantified at the DFT/BP/DN** level [29] the relative

acidities of SO_4/ZrO_2 and CF_3SO_3H and the basicities of pyridine and ethylenediamine (EDA) by calculating acid-base interaction energies. Reactants and products were fully optimized to rms gradient <0.0005 hartree/D. The SO_4/ZrO_2 catalyst site was modeled as $(HO)_3ZrOSO_3H$. The interaction energies are summarized in Table 11, which show that (1) SO_4/ZrO_2 (SZ) is a slightly stronger acid than CF_3SO_3H by 1.3-1.4 kcal/mol, (2) EDA is a stronger base than pyridine by 4.1-4.2 kcal/mol, and (3) the SO!H and H!N distances reflect the strength of the acid-base interaction.

Table 11. Energies (kcal/mol) of acid-base interactions and the SO!H!N distances (D)[a] derived from the computational models.

	BASE	
ACID	Pyridine	EDA
SZ	!18.54 (1.49, 1.10)	!22.72 (1.52, 1.09_6)
CH_3SO_3H	!17.23 (1.37, 1.16)	!21.29 (1.67, 1.07)
$(CH_3SO_3H)_2$[b]	-------	!21.61 (3.87, 1.04)[d]
$(CH_3SO_3H)_2$[c]	-------	!33.69 (1.12,1.44)[e]

[a]Entries in parentheses are the (SO!H distance, H!N distance) involving hydrogen between the SO! and !N= groups;
[b]EDA bound with one nitrogen to the acid group with hydrogen transfer;
[c]EDA bonded symmetrically to both acid groups;
[d]Only one of the two nitrogens is a proton acceptor; and
[e]Both nitrogens are bonded

PART III: A NOVEL STRONG ACID CATALYST

DESIGN AND SYNTHESIS

In the present work, a novel heterogeneous catalyst derived from a $(HO)_3Zr\text{-}O_3SOCH_2CH_2OSO_3\text{-}Zr(OH)_3$-type surface precursor was synthesized and studied. The precursor gave rise to proximal strong surface acid functionalities $(HOSO_2O\text{-}Zr\text{-}O\text{-})_2$ as prompted by the requirement that two alcohols need to be activated [11-13,30]. Complete characterization of the precursor salt, the synthsized catalyst precursor, and the calcined catalyst before and after use was carried out. The high resolution X-ray photoelectron (HR-XPS), near infrared (NIR) and ^{13}C magic angle spinning (MAS) nuclear magnetic resonance (NMR) spectra confirmed the composition, structure, and physicochemical properties of the catalyst. The results show that the 1,2-ethanediol, bis(hydrogen sulfate) moiety was successfully grafted onto the surface of zirconium hydroxide, as will be reported in detail in a subsequent publication when complete characterization of the catalyst has been accomplished. The main features of the preparation sequence are presented in the pictorial scheme that has been published [31].

In that scheme, the disodium 1,2-ethanediol bis(hydrogen sulfate) salt precursor **I** $\mathbf{(NaOSO_3CH_2)_2}$ obtained from Dr. Thomas H. Kalantar of the Dow Chemical Co. was converted to the ammonium form **II** $\mathbf{(NH_4OSO_3CH_2)_2}$ by exchange over a Rexyn 101 catex column. An aqueous solution of compound **II** was combined with an aqueous suspension of zirconium hydroxide to form the derivative **III** $\mathbf{(\text{-}O_xZr\text{-}OSO_3CH_2)_2}$. This solid was filtered, dried, and then calcined in air at 500EC to remove the $\text{–}(CH_2CH_2)\text{–}$ residues, resulting in the surface-derivatized species **IV** $\mathbf{(\text{-}O_xZr\text{-}OSO_3H)_2}$, corresponding to proximal

acid sites on zirconia. After the calcination treatment, this catalyst exhibited a surface sulfate-to-zirconium surface mole ratio of 0.84, corresponding to 0.72 mmol surface S/g cat., and all of the carbon from the precursor was removed. Thus, the final composition corresponds to the formula $(HSO_4)_{0.84}$-$ZrO_{2,surf}$ on the surface of pure zirconia. This material possessed a high thermal stability.

CATALYTIC RESULTS

The coupling/dehydration of methanol–isobutanol (2-methyl-1-propanol, 99.9+%, Alfa) was investigated in a downflow stainless steel tubular reactor with control of temperature (125-235EC), total pressure (101.3–3.1 x 10^3 kPa, 1 atm = 101.325 kPa) and i-BuOH/MeOH molar ratio (0/100–50/50) in a carrier gas of 5% N_2 diluted in He. The catalyst was centered in the vertical reactor in the heated zone by Pyrex beads above and below the bed. A J-type thermocouple was inserted into the top of the bed using an axial stainless steel thermowell. Product analyses were achieved with an on-line Hewlett-Packard gas chromatograph (Model 5890, Series II) equipped with automated heated sampling valves. A Cpsil-5CB capillary column was used.

Maintaining the methanol-isobutanol molar ratio = 1, the reaction temperature was varied. Table 12 shows that as the temperature was increased, the space time yield of MIBE significantly increased. Also observed were small quantities of dimethylether (DME), methyl tertiarybutyl ether (MTBE), diisobutyl ether (DIBE), and ditertiarybutyl ether (DTBE).

Table 12. Product space time yields (mol/kg cat/hr) in the reaction of MeOH/i-BuOH (1:1 molar ratio) with flow rates of 3.44 mol/kg cat/hr alcohols and 16 mol/kgcat/hr carrier gas at 101.3 kPa total pressure over the $(HO)_3Zr\text{-}O_3SOCH_2CH_2OSO_3\text{-}Zr(OH)_3$-derived catalyst.[a]

Temp. (EC)	MeOH Pressure (kPa)	i –BuOH Pressure (kPa)	MIBE	Isobutene	DME	MTBE	DIBE	DTBE	Octenes
125	8.97	8.97	0.002	----	----	----	----	----	—
150	8.97	8.97	0.020	----	----	----	0.008	----	0.004
175	8.97	8.97	0.087	1.430	----	----	0.005	0.003	0.005
175[b]	8.97	8.97	0.049	1.290[d]	0.103	0.007	----	----	----
175[c]	8.97	8.97	0.029	0.378[d]	0.034	0.014	0.015	0.016	----

[a] Steady state activities were readily achieved within 2 hr of initiating alcohol injection or after altering a reaction variable such as temperature. Extended testing of the $(HO)_3Zr\text{-}O_3SOCH_2CH_2OSO_3\text{-}Zr(OH)_3$–derived catalyst under each condition was performed for 8–12 hr. No catalyst deactivation was observed over several hundreds of hours of testing.
[b] SO_4^{2-}/ZrO_2 catalyst [14].
[c] H-montmorillonite catalyst [14; Table III].
[d] Butene included isobutene, n-butene, and cis- and trans-2-butene.

At 175EC, the MIBE yield was 0.087 mol/kg cat/hr, which represented an **enhancement of 78%** compared with 0.049 mol/kg cat/hr over previously reported SO_4^{2-}/ZrO_2 [14], and of 200% compared with 0.029 mol/kg cat/hr on an H-montmorillonite catalyst [14]. The isobutene yield of 1.43 mol/kg cat/hr, also observed at 175EC, represented an increase of 11% and ~280%, respectively, from 1.29 mol/kg cat/hr on SO_4^{2-}/ZrO_2 and 0.378 mol/kg cat/hr on H-montmorillonite catalyst [14].

Figure 19 shows the effect of i-BuOH addition on the production of dimethyl ether (DME) and MIBE. MIBE yields (■) increased and DME yields (●) decreased with increasing isobutanol partial pressure. When the ratio of i-BuOH/MeOH reached 12/88,

very little DME was observed, resulting in near-100% selectivity in favor of the unsymmetrical MIBE. This suggests that isobutanol suppressed the DME formation more effectively on this catalyst than on any of the previously studied catalysts [11-13,30].

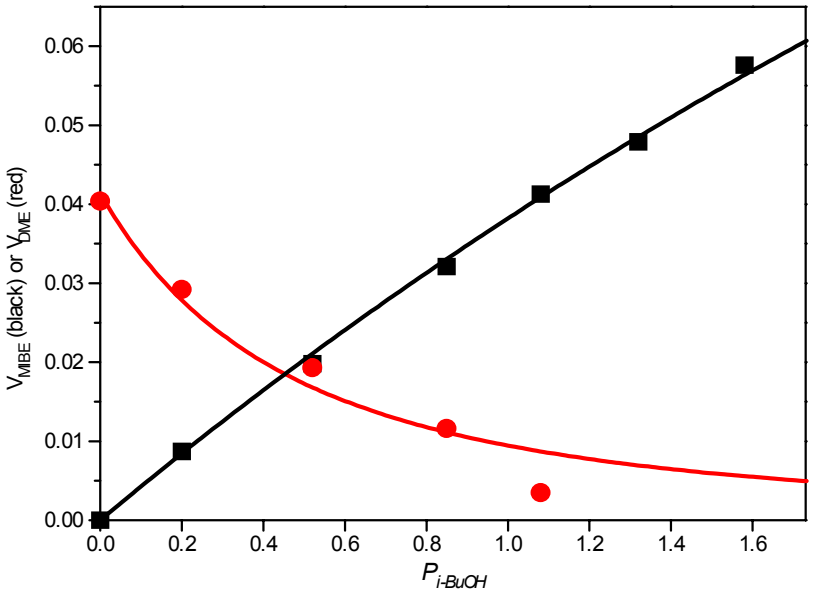

Figure 19. The effect of i-BuOH addition on DME (●) and MIBE (■) production. The abscissa axis is the partial pressure $P_{\text{I-BuOH}}$ in kPa at a constant pressure of methanol P_{MeOH} = 8.97 kPa. The ordinate axis expresses the rates of DME, v_{DME}, and MIBE, v_{MIBE}, in mol/kg cat/hr.

The adsorption constants of MeOH (K_M) and i-BuOH (K_B) were determined by curve fitting of the kinetic laws for the DME and MIBE formation [11-13]. K_B was derived to be 0.086 kPa^{-1} and K_M was found to be 0.035 kPa^{-1}. Here, the ratio $K_B/K_M = 2.46$ shows that isobutanol adsorbed preferentially on the acid sites, which agrees with its greater basicity over methanol [12,32]. The distribution of DME and MIBE in Figure 19 can be reasonably explained by kinetics previously observed on other catalysts [12], with $K_B > K_M$. The

experimental data also show increasing yields of isobutene with increased molar ratio of i-BuOH/MeOH. In addition, the enhancement of selectivity toward isobutene from 0% at 125EC to 94% at 175EC (Table 12) results from the increase of K_B/K_M with increasing temperature. The isobutanol dehydration to isobutene competed with MeOH/i-BuOH coupling to MIBE. At relatively high temperatures, a large ratio of K_B/K_M resulted in an enhancement of the $\theta_{i\text{-}BuOH}/\theta_{MeOH}$ ratio (θ, surface coverage), which favored the dehydration of the adsorbed isobutanol to isobutene (Equation 2). The apparent activation energy for the formation of each product was determined from Arrhenius plots, yielding 22 kcal/mol for MIBE and 24 kcal/mol for isobutene. The activation energy of 19 kcal/mol for DME was obtained by theoretical calculations [30].

Table 13 demonstrates that the MIBE yields at 175EC increased, whereas isobutene yields decreased with total alcohol pressure increasing from 7.8 to 240.7 kPa. For example, 0.156 mol/kg cat/hr MIBE at 7.8 kPa kept increasing with pressure to 0.702 mol/kg cat/hr at 240.7 kPa, while isobutene at 7.8 kPa (3.525 mol/kg cat/hr) exhibited a decreasing trend to 0.335 mol/kg cat/hr at 240.7 kPa.

The data in Table 13 are consistent with the Langmuir-Hinshelwood kinetic laws [12], $v_{MIBE} = k_4 K_M p_M K_B p_B/(1+K_M p_M+K_B p_B)^2$ (Equation 7) and $v_{Isobutene} = k_3 K_B p_B/(1+K_B p_B+K_M p_M)^2$ (Equation 6) that were derived on the basis of Reactions 1 and 2 occurring on dual acid sites [12]. The values of constants fitting the data of Table 13 were $k_3 = 33.1$ mol/kg cat/hr, $k_4 = 3.2$ mol/kg cat/hr, $K_M = 0.035$ kPa^{-1} and $K_B = 0.086$ kPa^{-1}.

Table 13. Product space time yields (mol/kg cat/hr) and selectivity (%) in the reaction of MeOH/i-BuOH (2:1 molar ratio) at 15.6 mol/kg cat/hr alcohols, 186 mol/kg cat/hr carrier gas and 175EC over $(HO)_3Zr\text{-}O_3SOCH_2CH_2OSO_3\text{-}Zr(OH)_3$-derived catalyst.[a]

Total pressure (kPa)	MeOH pressure (kPa)	i–BuOH pressure (kPa)	MIBE	Isobutene	DIBE	DTBE	MIBE selectivity (%)	Isobutene selectivity (%)
101.3	5.2	2.6	0.156	3.525	----	----	4.2	95.8
691.0	35.7	17.8	0.393	3.201	----	----	10.9	89.1
1036.5	53.5	26.7	0.521	2.972	----	0.012	14.9	84.8
1727.5	89.1	44.6	0.557	2.197	----	0.006	20.2	79.6
2418.5	124.8	62.4	0.675	1.473	----	0.007	31.3	68.4
3109.5	160.5	80.2	0.702	0.335	0.015	0.007	66.3	31.6

[a] Steady state activities were readily achieved within 2 hr of initiation of alcohol injection or after altering a reaction variable such as pressure. Extended testing of the $(HO)_3Zr\text{-}O_3SOCH_2CH_2OSO_3\text{-}Zr(OH)_3$-derived catalyst under each condition was carried out for 8–12 hr. No catalyst deactivation was observed over several hundred hours of testing.

The kinetic behavior of Equation 1 showed that isobutanol partial pressure (p_B) promoted the MeOH/i-BuOH coupling to MIBE, whereas the kinetic behavior of Equation 2 indicated that increasing isobutanol pressure (p_B) very strongly suppressed its dehydration, and the kinetic order became negative at high p_B [14]. At low alcohol partial pressures (p_M = 5.2 kPa and p_B = 2.6 pKa), high selectivity of isobutene (95%) is ascribed to a significant fraction of unoccupied acid sites on the surface of the $(HSO_4)_2\text{-}2ZrO_2$ catalyst. These free acid sites are considered to promote the dehydration of adsorbed isobutanol to isobutene according to the dual site elimination mechanism of Equation 2, whereby one site adsorbs the reacting alcohol and the second site is an acceptor for the product water [12,14]. At high alcohol partial pressures, the fraction of acid sites occupied by alcohol molecules approaches unity, and the catalyst favors MIBE formation. A maximum selectivity of MIBE reached 68% at 240 kPa total alcohol pressure (p_M = 160 kPa and p_B = 80 kPa) at the reaction

temperature of 175EC. The ratio of MIBE/isobutene increased with increasing alcohol pressure even at constant p_B/p_M. Moreover, the effect of pressure was found to be reversible, i. e. when alcohol pressure was decreased to its original value, isobutene production increased and MIBE decreased to their original rates.

The butene formed over the present $(HSO_4)_{0.84}$-$ZrO_{2,surf}$ catalyst was pure isobutene, whereas over other catalysts, such as H-montmorillonite and H-ZSM-5, products involved significant amounts of n-butene and cis- and trans-2-butene along with the isobutene. The highly concentrated Brr nsted acid sites on this catalyst effectively catalyzed removal of OH from the alcoholic carbon and of H from the neighboring carbon, resulting in isobutene formation. On the other hand, the single Brønsted acid site on the surface of other catalysts was associated with carbenium ion chemistry [33], which leads to butene rearrangement in isobutanol dehydration [33,34].

In conclusion, the novel heterogeneous catalyst derived form the $(HO)_3Zr$-$O_3SOCH_2CH_2OSO_3$-$Zr(OH)_3$ precursor effectively catalyzes MIBE formation at high pressures and favored isobutene production at low pressures.

CONCLUSIONS

With respect to the WO_3/ZrO_2 and Nafion-H catalysts under investigation in this research, the following conclusions can be made:

1. The tungstena/zirconia catalyst is active for coupling methanol and isobutanol to methylisobutylether (MIBE), but sideproducts are formed that consist mainly of isobutene, octenes, and dimethylether.
2. When the reaction temperature is increased above 135EC, the stable tungstena/zirconia catalyst is very good for dehydration of isobutanol to isobutene, even in the presence of methanol.
3. Ether and isobutene synthesis over the tungstena/zirconia catalyst could be described by Langmuir-Hinshelwood kinetics in which competitive adsorption of the two alcohols on surface Brønsted acid sites is a dominant feature and is consistent with a dual-site mechanism, similar to that previously described with Nafion-H [1,6], that proceeds *via* a S_N2 pathway.
4. The surface concentration of the accessible acid sites on the tungstena/zirconia catalyst is lower than expected from the tungstate content and are more diluted than observed with the Nafion-H catalyst.
5. The Brønsted acid sites on the tungstena/zirconia catalyst are heterogeneous since stronger amine bases detect (titrate) more Brønsted acid sites.
6. From the modelling study with the prototype sulfonic acid moiety, it is shown that the transition state barrier from the free reactants, . 16 kcal/mol, is comparable to the experimental 15 kcal/mol obtained with the Nafion-H resin [15,24].

In addition, a novel 1,2-ethanediol, bis(hydrogen sulfate), disodium salt precursor-based solid acid catalyst with a zirconia substrate was synthesized, and after calcination it was demonstrated to have significantly enhanced activity and high selectivity in producing methyl isobutyl ether (MIBE) or isobutene from methanol–isobutanol mixtures.

The results of this research have been published in the following publications to-date:

1. "Alcohol Coupling to Unsymmetrical Ethers over Solid Acid Catalysts," K. Klier, H.-H. Kwon, R. G. Herman, R. A. Hunsicker, Q. S. Ma, and S. J. Bollinger, in "*12th Intern. Congr. Catal.,"* Ed.: A. Corma, F. V. Melo, A. Mendioroz, and F. L. S. Fierro, Elsevier, Amsterdam, (2000) 3447.

2. "Synthesis of Unsymmetrical Ethers and Branched Olefins from Alcohols over a Novel $(HO)_3ZrO_3SO\text{-}CH_2CH_2\text{-}OSO_3ZR(OH)_3$-derived Catalyst," J. G. C. Shen, T. H. Kalantar, Q. Ma, R. G. Herman, and K. Klier, J. Chem. Soc., Chem. Commun. (2001) 653.

ACKNOWLEDGEMENTS

We thank Dr. Alfred C. Miller of the X-ray Photoelectron Spectroscopy Laboratory at Lehigh University for technical assistance with the XPS analyses of the catalysts. We thank Dr. Thomas H. Kalantar of the M.E. Pruitt Research Center, Dow Chemical Co., Midland, MI 48674 for providing the precursor salt that was used to prepare the novel sulfated zirconia catalyst having proximal strong HSO_4 surface acid sites.

REFERENCES

1. K. Klier, in "*Catalysis on the Energy Scene*," Ed.: A. Kaliaguine and A. Mahay, Elsevier, Amsterdam (1984) 439.

2. K. Klier, R. G. Herman, and C. W. Young, Preprints, Div. Fuel Chem., ACS, **29(5)** (1984) 273.

3. G. A. Vedage, P. B. Himelfarb, G. W. Simmons, and K. Klier, ACS Symp. Ser., **279** (1985) 295.

4. J. G. Nunan, C. E. Bogdan, K. Klier, K. J. Smith, C. W. Young, and R. G. Herman, J. Catal., **116** (1989) 195.

5. J. G. Nunan, R. G. Herman, and K. Klier, J. Catal., **116** (1989) 222.

6. E. Tronconi, N. Ferlazzo, P. Forzatti, and I. Pasquon, Ind. Eng. Chem. Res., **26** (1987) 2122.

7. E. Tronconi, L. Lietti, P. Forzatti, and I. Pasquon, Appl. Catal., **47** (1989) 317.

8. R. G. Herman, K. Klier, O. C. Feeley, and M. A. Johansson, Preprints, Div. Fuel Chem., ACS, **39(2)** (1994) 343.

9. T. H. Fleisch and P. C. Meurer, Fuel Technol. Manage., **6(4)** (1996) 54.

10. Y. Ohno, T. Shikada, T. Ogawa, M. Ono, and M. Mizuguchi, Preprints, Div. Fuel Chem., ACS, **42(2)** (1997) 705.

11. J. Nunan, K. Klier, and R. G. Herman, J. Chem. Soc., Chem. Commun. (1985) 676.

12. J. G. Nunan, K. Klier, and R. G. Herman, J. Catal., **139** (1993) 406.

13. O. C. Feeley, Q. Sun, R. G. Herman, M. A. Johansson, L. Lietti, and K. Klier, Catal. Lett., **35** (1995) 13.

14. K. Klier, R. G. Herman, M. A. Johansson, and O. C. Feeley, Preprints, Div. Fuel Chem., ACS, **37(1)** (1992) 236.

15. K. Klier, A. Beretta, Q. Sun, O. C. Feeley, and R. G. Herman, Catal. Today, **36** (1997) 3.

16. K. Klier, Q. Sun, O. C. Feeley, M. Johansson, and R. G. Herman, in *"Proc. 11th Intern. Congr. Catal.-40th. Ann.,"* (Studies in Surface Science and Catalysis), **101A**, ed. by J.W. Hightower, W.N. Delgass, E. Iglesia, and A.T. Bell, Elsevier, Amsterdam, 601 (1996).

17. L. Lietti, Q. Sun, R. G. Herman, and K. Klier, Catal. Today, **27** (1996) 151.

18. Q. Sun, R. G. Herman, and K. Klier, J. Chem. Soc., Chem. Commun., (1995) 1849.

19. J. G. Santiesteban, J. C. Vartuli, S. Han, R. D. Bastian, and C. D. Chang, J. Catal., **168** (1997) 431.

20. K. Klier, Catal. Rev., **1** (1967) 207.

21. G. F. A. Korteum, "*Reflectance Spectroscopy; Principles, Methods, Applications*," Engl. Translation by J. E. Lohr, Springer, NY (1969).

22. K. Klier, J. Opt. Soc. Am., **62** (1972) 882.

23. M. Johansson and K. Klier, Topics Catal., **4** (1997) 99 and M. Johansson, Ph.D. Dissertation, Department of Chemistry, Lehigh University (1995).

24. K. Klier, R. G. Herman, R. D. Bastian, S. DeTavernier, M. Johansson, M. Kieke, and O. C. Feeley, in "*Proc. Liquefaction Contractors' Review Meeting, U.S. Department of Engery-PETC*," ed. by G. J. Stiegel and R. D. Srivastava, Pittburgh, PA, 20-49 (1991).

25. J. H. Shen and K. Klier, J. Phys. Chem., **84** (1980) 1453.

26. J. H. Scofield, J. Electron Spectrosc. Relat. Phenom., **8** (1976) 129.

27. G. Beamson and D. Briggs, "*High Resolution XPS of Organic Polymers: The Scienta ESCA Database*," Wiley and Sons, Chichester, England (1992).

28. SPARTAN, ver. 3.1, Wavefunction, Inc., Irvine, CA, USA.

29. The DN** basis set uses polarization functions for hydrogen, is equivalent in performance to Gaussian 6-311G**, and its construction follows that in B. Delley, J. Chem. Phys., **92** (1990) 508 (Wavefunction, Inc., private communication).

30. K. Klier, H.-H. Kwon, R. G. Herman, R. A. Hunsicker, Q. S. Ma, and S. J. Bollinger, in "*12th Intern. Congr. Catal.,"* Ed.: A. Corma, F. V. Melo, A. Mendioroz, and F. L. S. Fierro, Elsevier, Amsterdam, (2000) 3447.

31. J. G. C. Shen, T. H. Kalantar, Q. Ma, R. G. Herman, and K. Klier, J. Chem. Soc., Chem. Commun. (2001) 653.

32. J. Long and B. Munson, J. Am. Chem. Soc., **95** (1973) 2427.

33. O. C. Feeley, M. A. Johansson, R. G. Herman, and K. Klier, Preprints, Div. Fuel Chem., ACS, **37(4)** (1992) 1817.

34. S. Kotsarenko and L. V. Malysheva, Kinet. Catal., **24** (1983) 877.